Received: 4 April 2023 | Revised: 15 March 2024 | Accepted: 20 March 2024

DOI: 10.1002/jev2.12430

RESEARCH ARTICLE

Transport of CLCA2 to the nucleus by extracellular vesicles controls keratinocyte survival and migration

Kristin Seltmann[1] | **Britta Hettich**[2] | **Seraina Abele**[1] | **Selina Gurri**[1] | **Valeria Mantella**[2] | **Jean-Christophe Leroux**[2] | **Sabine Werner**[1]

[1]Institute of Molecular Health Sciences, Department of Biology, Swiss Federal Institute of Technology (ETH) Zurich, Zurich, Switzerland

[2]Department of Chemistry and Applied Biosciences, Institute of Pharmaceutical Sciences, ETH Zurich, Zurich, Switzerland

Correspondence
Kristin Seltmann and Sabine Werner, Institute of Molecular Health Sciences, ETH Zurich, 8093 Zurich, Switzerland.
Email: kristin.seltmann@biol.ethz.ch and sabine.werner@biol.ethz.ch

Abstract

Chloride channel accessory 2 (CLCA2) is a transmembrane protein, which promotes adhesion of keratinocytes and their survival in response to hyperosmotic stress. Here we show that CLCA2 is transported to the nucleus of keratinocytes via extracellular vesicles. The nuclear localization is functionally relevant, since wild-type CLCA2, but not a mutant lacking the nuclear localization signal, suppressed migration of keratinocytes and protected them from hyperosmotic stress-induced cell death. In the nucleus, CLCA2 bound to and activated β-catenin, resulting in enhanced expression of Wnt target genes. Mass-spectrometry-based interaction screening and functional rescue studies identified RNA binding protein 3 as a key effector of nuclear CLCA2. This is of likely relevance in vivo because both proteins co-localize in the human epidermis. Together, these results identify an unexpected nuclear function of CLCA2 in keratinocytes under homeostatic and stress conditions and suggest a role of extracellular vesicles and their nuclear transport in the control of key cellular activities.

KEYWORDS

cell death, CLCA2, extracellular vesicles, hyperosmotic stress, keratinocytes, migration, nuclear transport, RBM3, β-catenin

1 | INTRODUCTION

The skin as the outermost surface of the body provides an essential barrier, which protects from invasion of pathogens, irritants and allergens and from excessive water loss (Proksch et al., 2008). Maintenance of skin integrity and its barrier function require a tight connection between keratinocytes, the major cell type of the epidermis. Alterations of cell-cell contacts can affect central processes, including keratinocyte proliferation, migration and survival. Impaired keratinocyte adhesion is therefore a hallmark of major inflammatory skin diseases, such as atopic dermatitis and psoriasis (Chung et al., 2005; Furukawa et al., 1994; Proksch et al., 2006).

We recently identified an important role of the transmembrane protein "chloride channel accessory 2" (CLCA2) in keratinocyte adhesion (Seltmann et al., 2018). CLCA2 is one of three functional members of the human CLCA family, which were initially discovered as possible regulators of chloride channel activity. CLCA2 is mainly known for its tumour suppressive function in breast cancer, where it inhibits cell migration and invasion (Sasaki et al., 2012; Walia et al., 2012). CLCA2 expression increased in nucleus pulposus cells and keratinocytes in response to hyperosmotic stress (Mavrogonatou et al., 2015; Seltmann et al., 2018). This stress condition is present in the skin of patients with impaired epidermal barrier function, in particular in a dry environment. Consistently, CLCA2 is overexpressed in the epidermis of patients suffering from Atopic Dermatitis (Seltmann et al., 2018),

most likely as a compensatory mechanism. The increased CLCA2 levels in keratinocytes are important for the stabilization of cell-cell contacts as demonstrated by the reduced adhesive strength of cultured keratinocytes with CLCA2 knock-down (Seltmann et al., 2018). Consistent with a role of CLCA2 in cell-cell contact formation, it was shown to interact with the cell adhesion protein EVA-1 in breast cancer cells and with β-catenin, a component of adherens junctions, when overexpressed in HEK 293T cells (Ramena et al., 2016).

Small amounts of β-catenin are also present in the nucleus under homeostatic conditions. β-catenin gets stabilized and accumulates in this compartment in the presence of Wnt ligands or when components of the β-catenin destruction complex are mutated or down-regulated through other mechanisms. Nuclear β-catenin regulates the expression of Wnt target genes upon interaction with TCF transcription factors (Mosimann et al., 2009).

Here we show that CLCA2 is secreted from keratinocytes via extracellular vesicles (EVs). CLCA2-containing EVs were taken up by keratinocytes and other cell types and were detected in the cytoplasm and also in the nucleus of the recipient cells. This finding identifies an unexpected and poorly characterized EV-mediated transport mechanism that allows targeting of transmembrane proteins to the nucleus. In this compartment, CLCA2 interacted with β-catenin, RNA binding protein 3 (RBM3) and additional regulators of gene expression. This is functionally relevant, because only CLCA2 with a nuclear localization sequence promoted expression of Wnt target genes in keratinocytes, enhanced the survival of these cells under hyperosmotic stress conditions and suppressed their migration. Together with the co-expression of CLCA2 and RBM3 in the epidermis of human skin, these findings suggest key roles of CLCA2 and its interactors in the control of gene expression in the epidermis.

2 | MATERIALS AND METHODS

2.1 | Human skin samples

Human foreskin was obtained anonymously and upon written consent from the parents in the context of the biobank project of the Department of Dermatology, University of Zurich. The experiments were conducted in conformity to the principles set out in the WMA Declaration of Helsinki and the Department of Health and Human Services Belmont Report. The use of samples for research purpose was approved by the local ethics commission (KEK Nr. 2017-00684).

2.2 | Generation of a CLCA2 mutant lacking the nuclear localization signal (NLS)

The CLCA2 cDNA was amplified from a pCMV6-XL4 cDNA-containing bacterial glycerol stock (OriGen Technologies, Inc., Rockville, MA; SC116023) and cloned into the pENTR/D-TOPO entry vector (Thermo Fisher Scientific, Waltman, MA; K240020). A Q5 Site-Directed Mutagenesis kit (New England Biolabs, Ipswich, MA; E0554S) was used to generate the NLS mutation. The coding sequence of mutated *CLCA2* was inserted into the pInducer20 destination vector (kindly provided by Dr. S. Elledge, Harvard University Medical School, Boston) using the Gateway LR Clonase II Enzyme mix (Thermo Fisher Scientific; 11791019).

2.3 | Cell culture and transfection

HaCaT keratinocytes (immortalized human keratinocytes (Boukamp et al., 1988)) and HEK 293T cells were cultured in Dulbecco's modified Eagle's Medium (DMEM; Sigma–Aldrich, St. Louis, MO) supplemented with 10% foetal bovine serum (FCS; Thermo Fisher Scientific) and penicillin/streptomycin (P/S; Sigma–Aldrich). Stably transfected cell lines were maintained in the same medium, which was supplemented with 100 µg/mL puromycin (Sigma–Aldrich). In some experiments, cells were treated with 10 ng/mL leptomycin B (LMB) (Enzo Life Sciences, Farmingdale, NY), 10 µM brefeldin A or 10 µg/mL heparin. Absence of mycoplasma was confirmed by PCR using the PCR Mycoplasma Test Kit I/C (PromoKine, Heidelberg, Germany).

HaCaT keratinocytes stably transduced with lentiviruses allowing expression of CLCA2 shRNA in a docycycline (Dox)-inducible manner were previously described (Seltmann et al., 2018). For all experiments in this manuscript, they were treated for 2 days with 1 µg/mL Dox unless indicated otherwise. For DNA plasmid transfection, the Xfect transfection reagent (Takara Bio, Shiga, Japan) was used according to the manufacturer's protocol. For siRNA transfection, cells were transfected with Xfect RNA transfection reagent (Takara Bio) and analysed 48 h later.

The following siRNA sequences were used:

Gene	siRNA
CLCA2	UGACAAACCUUUCUACAUA
RBM3-1	GTGGATCATGCAGGCAAGT
RBM3-2	GGTGGTTATGACCGCTACT
RBM3-3	CCAAATGGCTGTATTTATAAA
KPNB1-1	GCUCAAACCACUAGUUAUA
KPNB1-2	GACGAGAAGUCAAGAACUA
KPNB1-3	GGGCGGAGAUCGAAGACUA
RanBP2	CCGUUUUGGUGAGUCAACA

For treatment of cells with EVs, cells were grown to confluency, starved overnight in serum-free media, and incubated with purified EVs for different time periods.

2.4 | Cell migration assay

HaCaT cells were seeded into 12-well plates, transfected with siRNAs or expression vectors, and grown to 100% confluency. They were cultured in DMEM/10% FBS/1% P/S and treated with mitomycin C (2 μg/mL; Sigma–Aldrich) for 2 h at 37°C. A scratch was made vertically from the top to the bottom of each well using a sterile P200 pipette tip. The medium was aspirated, and cells were washed with PBS. Normal culture medium was added, and the scratched area was photographed and analysed at different time points.

2.5 | LDH cytotoxicity assay

LDH assay was performed using a Pierce LDH Cytotoxicity Assay Kit (Thermo Fisher Scientific; 88953) according to the manufacturer's instructions. Colorimetric measurements at 490 and 600 nm were performed using a GloMax Discoverer plate reader (Promega, Madison, WI).

2.6 | MTT assay

Cells were seeded into 12-well plates (2×10^4 cells/well) and transfected. After treatment with 200 mM sorbitol for 24 h, 150 μL MTT (Abcam; ab146345) solution (5 mg/mL 3-(4,5-dimethylthiazol-2-yl)-2,5-diphenyltetrazolium bromide (MTT) in PBS) was added to each well and incubated for 30 min. The supernatant was aspirated, and the cells were lysed with 225 μL MTT lysis buffer (49.5 μL HCl in 15 mL isopropanol) for 10 min at room temperature (RT). 100 μL were transferred to a 96-well plate, and the absorption was measured at 600 nm using a GloMax Discoverer plate reader.

2.7 | RNA isolation and quantitative RT-PCR

Total RNA from cultured cells was purified using an RNA isolation kit (IBI Scientific, Dubuque, IA), including DNase treatment, according to the manufacturer's instructions. RNA was reverse transcribed using the iScript cDNA synthesis kit (BioRad, Hercules, CA). Relative gene expression was determined using the LightCycler 480 SYBR Green system (Roche, Rotkreuz, Switzerland). Gene expression was normalized to the housekeeping gene ribosomal protein L27 (*RPL27*), and the mean of the control group was set to 1. Primer sequences are listed below.

The following primers were used:

Gene	Forward primer (5′−3′)	Reverse primer (5′−3′)
RPL27	TCA CCT AAT GCC CAC AAG GTA	CCA CTT GTT CTT GCC TGT CTT
CLCA2	ACT GTG GGC AAC GAC ACT AT	GTC CAG TGC CCA GGC TTA
AXIN2	TAC ACT CCT TAT TGG GCG ATC A	TTG GCT ACT CGT AAA GTT TTG GT
MYC	TGA GGA GAC ACC GCC CAC	CAA CAT CGA TTT CTT CCT CAT CTT C
CCND1	ACG AAG GTC TGC GCG TGT T	CCG CTG GCC ATG AAC TAC CT
BMP4	ATG ATT CCT GGT AAC CGA ATG C	CCC CGT CTC AGG TAT CAA ACT
CTGF	AAA AGT GCA TCC GTA CTC CCA	CCG TCG GTA CAT ACT CCA CAG
RBM3	ACC ATC CAG AGA CTC TCC GT	CTT CAG CAG TTT CGG ACC TA
CTNNB1	TGG ATG GGC TGC CTC CAG GTG AC	ACC AGC CCA CCC CTC GAG CCC

2.8 | Preparation of cell lysates and western blot analysis

Preparation of cell lysates and western blotting were described previously (Seltmann et al., 2013). Nuclear, cytoplasmic and membrane fractions were separated by different centrifugation steps (Seltmann et al., 2015). Briefly, cells were lysed in lysis buffer (20 mM Tris, pH 7.5, 5 mM EDTA, 2 mM EGTA) supplemented with fresh Pierce protease inhibitor tablet (Thermo Fisher Scientific) and incubated for 30 min on a shaker at 4°C. The cytosolic fraction was present in the supernatant after centrifugation at 16,000×g for 1 h. The pellet was solubilized in resuspension buffer (1% Triton X-100, 20 mM Tris, pH 7.5, 5 mM EDTA, 2 mM EGTA, and fresh protease inhibitor cocktail), incubated for 30 min at 4°C, and centrifuged again (16,000×g for 1 h). The supernatant represents the membrane fraction. 2× Laemmli sample buffer was added to all samples before analysing them by western blotting.

For precipitation of proteins from the serum-free cell supernatant, pre-cooled acetone (−20°C; four volumes of the supernatant) was added, and the mixture was incubated for 3 h at −20°C. Samples were centrifuged for 30 min at 13,000×g. The supernatant was removed, and the remaining acetone was evaporated for 30 min at room temperature. The pellet was dissolved in sample buffer and used for Western blot analysis.

The following antibodies were used:

Antibody	Company	DILUTION	ORDERING NUMBER
Rabbit anti-CLCA2	Sigma–Aldrich	1:1000	HPA047192
Mouse anti-β-catenin (total)	Sigma–Aldrich	1:5000	clone 15B8
Rabbit anti-active β-catenin	Cell Signalling, Danvers, MA	1:1000	D2U8Y
Mouse anti-E-cadherin	BD Biosciences, Franklin Lakes, NJ	1:5000	610181
Mouse anti-RBM3	Sigma–Aldrich	1:1000	AMAB90655
Mouse anti-tubulin	Sigma–Aldrich	1:10000	clone B-5-1-2
Rabbit anti-histone H1	Abcam, Cambridge, UK	1:5000	EPR6536 (ab134914)
Mouse anti-epidermal growth factor receptor (EGFR)	Santa Cruz Biotechnology, Santa Cruz, CA	1:1000	sc-03-G (1005)
Mouse anti-caveolin-1	Santa Cruz Biotechnology	1:1000	sc-894
Mouse anti-TSG101	Santa Cruz Biotechnology	1:1000	sc-7964
Mouse anti-calreticulin	Santa Cruz Biotechnology	1:1000	sc-373863
Mouse anti-CD9	Santa Cruz Biotechnology	1:1000	sc-13118
Mouse anti-CD63	Santa Cruz Biotechnology	1:1000	sc-5275
Anti-mouse IgG-HRP	Promega	1:10000	W4021
Anti-rabbit IgG-HRP	Promega	1:10000	W4011

2.9 | Co-immunoprecipitation (Co-IP)

Confluent cells were washed with PBS and lysed with RIPA buffer (10 mM Na_2HPO_4, 150 mM NaCl, 5 mM EDTA, 2 mM EGTA, 1% Triton X-100, 0.25% SDS, 1% sodium deoxycholate, 0.1 mM DTT, pH 7.5) supplemented with Pierce protease and phosphatase inhibitor tablet (Thermo Fisher Scientific). Lysates were incubated for 30 min at 4°C and centrifuged at 16,000×g for 10 min at 4°C. Supernatants were pre-cleared with 30 µL Dynabeads Protein G (Thermo Fisher Scientific) and incubated for 1 h at 4°C. The specific antibody or IgG control was added to cell lysates at a concentration of 1 µg antibody per 0.5 mg protein lysate and incubated overnight at 4°C. Dynabeads Protein G were added, and the samples were incubated under rotation at 4°C for 3 h. After several washing steps, bead-bound proteins were eluted by addition of sample buffer, heated for 15 min at 95°C and analysed by western blotting.

2.10 | IP from nuclear lysates and mass spectrometry (MS) analysis

Nuclear extracts were prepared using the nuclear complex Co-IP kit (Active Motif Inc., Carlsbad, CA) according to the manufacturer's instructions. 500 µg nuclear protein lysate was used for IP and incubated with 3 µg antibody in a total volume of 500 µL overnight at 4°C. On the following day, 30 µL Dynabeads Protein G (Thermo Fisher Scientific) were added to the lysate and incubated for 2 h under rotation at 4°C. Beads where then washed three times using High buffer (Active Motif kit). Proteins bound to the beads were directly analysed by Western blot or digested overnight with trypsin (100 ng/µL), followed by on-bead digestion and MS analysis using a nanoAcquity ultraperformance liquid chromatography (UPLC) system (Waters Inc., Milford, MA) coupled to a Q-Exactive mass spectrometer (Thermo Fisher Scientific).

2.11 | Sample preparation for protein quantification

Five hundred microgram nuclear protein lysate was used for IP and incubated with 3 µg antibody in a total volume of 500 µL overnight at 4°C. On the following day, 30 µL Dynabeads Protein G (Thermo Fisher Scientific) was added to the lysate and incubated for 2 h under rotation at 4°C. Beads were then washed three times using High buffer (Active Motif Inc.). Proteins bound to the beads were directly analysed by Western blot or digested as follows: For each sample, the beads were washed once with 100 µL of digestion buffer (10 mM Tris/2 mM $CaCl_2$, pH 8.2). The washed beads were re-suspended in 45 µL digestion buffer, and the proteins were on-bead digested using 5 µL of sequencing grade trypsin (100 ng/µL in 10 mM HCl, Promega). The digestion was carried out in a microwave instrument (Discover System, CEM Corporation, Matthews, NC) for 30 min at 5 W and 60°C. The supernatants were transferred into new tubes, and the beads were additionally digested for 3 h at room temperature. The beads were washed with 100 µL trifluoroacetic acid (TFA) buffer (0.1% TFA/10 mM Tris/2 mM $CaCl_2$), and the supernatants were collected and combined with the previously collected one. The samples were finally dried in a speed-vac, resolubilized in 20 µL of 0.1% formic acid and centrifuged at 20,000 g for 10 min. Samples were further diluted 1:5 in 0.1% formic acid, and 10 µL were transferred into liquid chromatography—mass spectrometry (LC-MS) vials.

2.12 | LC-MS/MS analysis

LC-MS/MS analysis was performed on a nanoAcquity UPLC system (Waters Inc.) connected to a Q Exactive mass spectrometer (Thermo Scientific) equipped with a Digital PicoView source (New Objective Inc., Littleton, MA). Solvent composition at the two channels was 0.1% formic acid for channel A and 0.1% formic acid, 99.9% acetonitrile for channel B. For each sample, 1 µL was injected. Peptides were trapped on a Symmetry C18 trap column (5 µm, 180 µm×20 mm, Waters Inc.) and separated on a BEH300 C18 column (1.7 µm, 75 µm×150 m, Waters Inc.) at a flow rate of 300 nL/min using a gradient from 5% to 35% B in 90 min, 60% B in 5 min and 80% B in 1 min. The mass spectrometer was operated in data-dependent mode (DDA), acquiring full-scan MS spectra (350−1500 m/z) at a resolution of 70.000 at 200 m/z after accumulation to a target value of 3.000.000, followed by higher-energy collision dissociation (HCD) fragmentation on the twelve most intense signals per cycle. HCD spectra were acquired at a resolution of 35.000 using a normalized collision energy of 25 units and a maximum injection time of 120 ms. The automatic gain control (AGC) was set to 50000 ions. Charge state screening was enabled, and singly and unassigned charge states were rejected. Only precursors with intensity above 25,000 were selected for MS/MS. Precursor masses previously selected for MS/MS measurement were excluded from further selection for 40 s, and the exclusion window was set at 10 ppm. The samples were acquired using internal lock mass calibration on m/z 371.1010 and 445.1200.

2.13 | MS/MS data analysis

Raw data were converted into Mascot Generic Format files (.mgf) using ProteoWizard (http://proteowizard.sourceforge.net/), and the proteins were identified using the Mascot search engine (Matrix Science, London, UK; version 2.6.2). Spectra were searched against a Swissprot human canonical proteome database (taxonomy 9606, version from 2019-07-09), concatenated to its reversed decoyed fasta database. Methionine oxidation was set as variable modification, and enzyme specificity was set to trypsin, allowing a maximum of two missed cleavages. A fragment ion mass tolerance of 0.030 Da and a parent ion tolerance of 10.0 PPM were set. Scaffold (Proteome Software Inc., Portland, OR; version 4.11) was used to validate MS/MS-based peptide and protein identifications. Only proteins with Scaffold Local probabilities equal or higher than 99.0% were retained for analysis (two or more peptides per protein contributing to a positive match). Computation of putative PPIs (manual and SAINTexpress (Teo et al., 2014)) were based on exclusive spectrum counts as determined by Scaffold.

2.14 | Immunofluorescence staining and proximity ligation assay

Conditions for immunostaining and image processing were described previously (Seltmann et al., 2015). Briefly, cells were fixed for 10 min in 4% paraformaldehyde in PBS and incubated with primary antibodies overnight at 4°C. All antibodies were diluted in TBS containing 1% BSA. After washing, the diluted secondary antibodies were applied and incubated for 1 h. Nuclei were counterstained with Hoechst. Images were acquired using an Imager.A1 microscope equipped with an enhanced-contrast Plan-Neofluar objective (63x/1.4NA) and photographed with an Axiocam MRm camera (all from Carl Zeiss, Inc., Oberkochen, Germany). Data analysis was performed using Zen 2.3 lite software (Carl Zeiss, Inc.) and ImageJ v1.48 software (National Institutes of Health, Bethesda, MD).

Proximity ligation assays (PLA) were performed according to the manufacturer's instructions (Duolink PLA; Sigma–Aldrich) using primary rabbit and mouse antibodies. Donkey anti-mouse secondary antibody conjugated to oligonucleotide (minus; DUO92004; Sigma–Aldrich) and donkey anti-rabbit secondary antibody conjugated to oligonucleotide (plus; DUO92002; Sigma–Aldrich) were used. Fluorescence was detected using a Zeiss LSM 880 Airyscan microscope equipped with a 63 × 1.4NA Oil DIC Plan-Apochromat objective (Carl Zeiss, Inc.). All images in a given experiment were taken under identical imaging parameters in sequential scan mode. 3D modelling of the surface of the nucleus was performed based on the confocal images acquired after Hoechst staining, and fluorescence-labelled EVs and CLCA2 immunofluorescence staining were visualized with spot detection and surface function of Imaris 9.5 software (Oxford Instruments, Abingdon, UK).

The following antibodies/reagents were used:

Antibody/Reagent	Company	DILUTION	ORDERING NUMBER
Alexa Fluor 594 AffiniPure donkey anti-mouse IgG (H+L)	Jackson ImmunoResearch, West Grove, PA	1:500	#715-545-150
Alexa Fluor 488 AffiniPure donkey anti-rabbit IgG (H+L)	Jackson ImmunoResearch	1:500	#711-547-003
Alexa Fluor 594 AffiniPure donkey anti-rabbit IgG (H+L)	Jackson ImmunoResearch	1:500	#711-587-003
Hoechst 33342 (B2261)	Sigma–Aldrich	1:1000	#A34055
Rabbit anti-CLCA2	Sigma–Aldrich	1:200	#HPA047192
Mouse anti-β-catenin (total)	Sigma–Aldrich	1:200	clone 15B8; #14-2567-82
Mouse anti-E-cadherin	BD Biosciences, Franklin Lakes, NJ	1:500	#610181
Mouse anti-RBM3	Sigma–Aldrich	1:100	#AMAB90655

2.15 | Purification of EVs

EVs were purified from serum-free supernatant of cells at 80% confluency using a two-step centrifugation procedure as previously described (Hettich et al., 2020). The supernatant was first centrifuged at 2000×g for 5 min and then at 10,000×g for 15 min at 4°C, followed by filtration of the supernatant through a 0.2 µm pore-sized filter (TPP Techno Plastic Products AG, Trasadingen, Switzerland). EVs were then pelleted at 100,000×g and 4°C for 70 min using an Optima XE-90 centrifuge (Beckman Coulter Life Sciences, Brea, CA). After washing with PBS, the EVs were centrifuged again under the same conditions. The EV pellet

was resuspended in PBS, and the protein concentration was measured using the Micro BCA Protein Assay Kit (Thermo Fisher Scientific).

2.16 | Nanoparticle tracking analysis (NTA)

EV sizes were determined by NTA on a PMX 120 ZetaView (Particle Metrix GmbH, Inning, Germany) equipped with a 405 nm laser and a CMOS camera (Kopp et al., 2020). The Zetaview machine was calibrated with polystyrene beads (Sigma–Aldrich), diluted 1:500,000 at a concentration of around 100 particles per frame. The measurements were performed by applying a bin size width of 5 nm/class, a minimum brightness of 25, a minimum area of 5, a maximum area of 1000, and a trace length of 15, and shutter was set to 150, the sensitivity to 85, and the frame rate to 30 per second. All EV samples were measured in triplicates. The ZetaView software version 8.04.04 SP2 was used.

2.17 | Labelling of EVs

EV membrane proteins were labelled using DyLight 650 or DyLight 594 NHS ester (Thermo Fisher Scientific). The dye solution was mixed with the EVs in a 20:1 vesicle/dye ratio (μg/μg) and incubated under rotation for 2 h at 4°C, followed by incubation for 2 h at RT. To remove excess dye from the EVs, Zeba Spin Desalting Columns, 40 K MWCO (Thermo Fisher Scientific), were used according to the manufacturer's instructions, followed by several PBS washes. Alternatively or in addition, EVs were incubated with CellTrace dye (Thermo Fisher Scientific) at a final concentration of 5 μM and incubated at 4°C overnight. On the following day, EV samples were incubated at 37°C for 15 min to allow the reagent to undergo acetate hydrolysis. Stained EVs were dialyzed using Pur–A–Lyzer tubes (Sigma–Aldrich) overnight at 4°C following the manufacturer's instructions.

2.18 | Transmission electron microscopy analysis of EVs

For transmission electron microscope (TEM) imaging, DyLight −594 labelled EV-samples were purified as described above. Five microlitre of sample was placed on glow discharged (Pelco, Ted Pella, Redding, CA) carbon-coated grids (Quantifoil, Grossl̈obichau, Germany) and incubated for 3 min. After this interval, excess fluid was removed with filter paper and the grid was washed twice. The wet sample was stained in a drop of 2% uranyl acetate for 1 s followed by a second step for 15 s. Excess moisture was drained with filter paper, and the imaging of the air-dried grids was done in a TEM Morgagni 268 (Thermo Fisher Scientific) operated at 100 kV acceleration voltage. Data were acquired with a KeenView CCD-camera (Soft Imaging System, Muenster, Germany; 1376 × 1032 Pixel). In addition, EV samples were imaged using a Tecnai F20 field emission gun (FEG) microscope (Field Electron and Ion Company, Hillsboro, OR), operated at a 120 kV acceleration voltage, and equipped with a combination of CCD (ORIUS SC200 2 K) and direct electron detector (Falcon II 4 K, Thermo Fisher Scientific).

2.19 | Luciferase reporter assays

Cells were co-transfected with the TCF/LEF firefly luciferase reporter plasmid and a β-actin-Renilla reporter plasmid for normalization. M50 Super 8x TOPFlash was obtained from Addgene, Watertown, MA (plasmid # 12456; http://n2t.net/addgene:12456; RRID:Addgene_12456; made available by Dr. Randall Moon (Veeman et al., 2003)). The activities of Firefly luciferase encoded by the promoter plasmid and of Renilla luciferase were analysed using the Dual-Glo dual-luciferase reporter assay system (Promega) according to the manufacturer's instructions.

2.20 | Statistical analysis

Statistical analysis was performed with the Prism9 software (GraphPad Software Inc, San Diego, CA). Quantitative data are expressed as mean ± S.E.M. Significance was calculated using two-way ANOVA for multiple comparisons; $^{*}p \leq 0.05$, $^{**}p \leq 0.01$, $^{***}p \leq 0.001$, $^{****}p \leq 0.0001$.

3 | RESULTS

3.1 | CLCA2 is present at the plasma membrane and in the nucleus of keratinocytes

CLCA2 has a cytoprotective function in keratinocytes, which is, at least in part, mediated through its effect on cell-cell contacts (Seltmann et al., 2018). However, its molecular mechanisms of action are only partially understood. To further characterize this protein, we cloned expression vectors that allow the production of CLCA2 fusion proteins with an amino-terminal influenza hemagglutinin (HA)-tag that was inserted in-frame between the signal peptide and the mature protein or with a carboxy-terminal FLAG-tag (Figure 1a). The full-length CLCA2 protein is glycosylated, resulting in the production of a protein with an apparent molecular weight of 120–130 kDa. It can undergo auto-cleavage (Elble et al., 2006), giving rise to a secreted cleavage product of ~85 kDa and a transmembrane fragment of ~35 kDa (Figure 1b). The fusion proteins were expressed in HEK 293T cells, which do not express endogenous CLCA2 (Seltmann et al., 2018). Expression of the full-length glycosylated fusion proteins was confirmed by Western blot (Figure 1c). The HA antibody also detected bands between 55 and 100 kDa, which may represent additional cleavage products. A 35 kDa protein was detected with the anti-FLAG antibody, which most likely represents the C-terminal cleavage product. Western blot analysis of membrane, cytoplasmic and nuclear fractions confirmed the presence of CLCA2 and its C-terminal cleavage product in the membrane, while it was hardly detectable in the cytoplasm. Surprisingly, it was also detected in the nuclear fraction (Figure 1d), and this was confirmed by immunofluorescence staining, where some cells showed nuclear staining (Figure 1e). These results are consistent with data from the Human Protein Atlas, which showed nuclear staining of CLCA2 in HaCaT keratinocytes and immortalized corneal epithelial cells (https://www.proteinatlas.org/ENSG00000137975-CLCA2/cell). The nuclear levels increased when keratinocytes were treated for 4 h with the nuclear export inhibitor leptomycin B (LMB) (Figures 1e and S1a). Because both full-length CLCA2 and its C-terminal cleavage product have a transmembrane domain, they are most likely located in the nuclear membrane.

Translocation of CLCA2 to the nucleus requires its unique nuclear localization site (NLS) present in the intracellular C-terminal part of the protein, since only expression of a FLAG-tagged wild-type (WT) protein (CLCA2-WT), but not of CLCA2 with a point mutation in the NLS (CLCA2-ΔNLS), enhanced the levels of nuclear CLCA2 in transfected HaCaT cells (Figure S1b). Of note, CLCA2-ΔNLS was expressed at similar levels as CLCA2-WT (Figure S1b). Furthermore, both the wild-type and the mutant protein interacted at the plasma membrane with the previously identified CLCA2 binding partners E-cadherin and β-catenin (Ramena et al., 2016; Seltmann et al., 2018) as revealed by co-immunoprecipitation (Figure S1c), suggesting proper localization and folding of CLCA2-ΔNLS. Immunofluorescence staining of LMB-treated cells confirmed the increase in nuclear CLCA2 upon overexpression of CLCA-WT in HaCaT cells, while CLCA2-ΔNLS did not accumulate in the nucleus (Figures 1f and S1d). siRNA-mediated knock-down of importin β1 (KPNB1) or Ran binding protein 2 (RanBP2) (Figures S1e and S1f), which are required for entry of proteins into the nucleus through the nuclear pore (Walde et al., 2012), strongly reduced the levels of nuclear CLCA2 (Figure 1 g) and its total intracellular levels (Figure S1e).

3.2 | Nuclear CLCA2 promotes keratinocyte survival under hyperosmotic stress conditions and suppresses migration

CLCA2 is required for keratinocyte survival in response to hyperosmotic stress, which can be induced by treatment with sorbitol or high salt (Seltmann et al., 2018). Interestingly, this activity requires the presence of CLCA2 in the nucleus, since the low survival rate of sorbitol-treated HaCaT cells with CLCA2 knock-down was rescued by overexpression of CLCA2-WT, but not of CLCA2-ΔNLS (Figure 1h). Furthermore, overexpression of CLCA2-WT in HaCaT cells reduced cell migration, while CLCA2-ΔNLS did not have this activity. Vice versa, shRNA-mediated CLCA2 knock-down promoted keratinocyte migration. The increased migration was fully reversed upon transient overexpression of CLCA2-WT, while overexpression of the CLCA2-ΔNLS mutant caused only a partial rescue (Figures 1i). Figure S1h schematically shows the workflow in this and the following experiments that involve a combination of knock-down and overexpression.

3.3 | EVs contain CLCA2 that can be transported to nucleus

The surprising localization of a transmembrane protein in the nucleus raised the question about the trafficking of this protein. Previous studies showed a role of endosomes in the transport of plasma membrane proteins to the nucleus, which may involve retrograde trafficking via the Golgi apparatus and the endoplasmic reticulum (ER) (Chen et al., 2020) or a direct interaction of endosome-derived vesicles with the outer nuclear membrane or the nuclear pore complex (Shah et al., 2019). Another possibility is the transport via EVs (Corbeil et al., 2020). EVs are single-membrane vesicles that are released from various mammalian cells and contain several transmembrane proteins (Chavez-Munoz et al., 2008; Mathivanan et al., 2010). Consistent with a potential

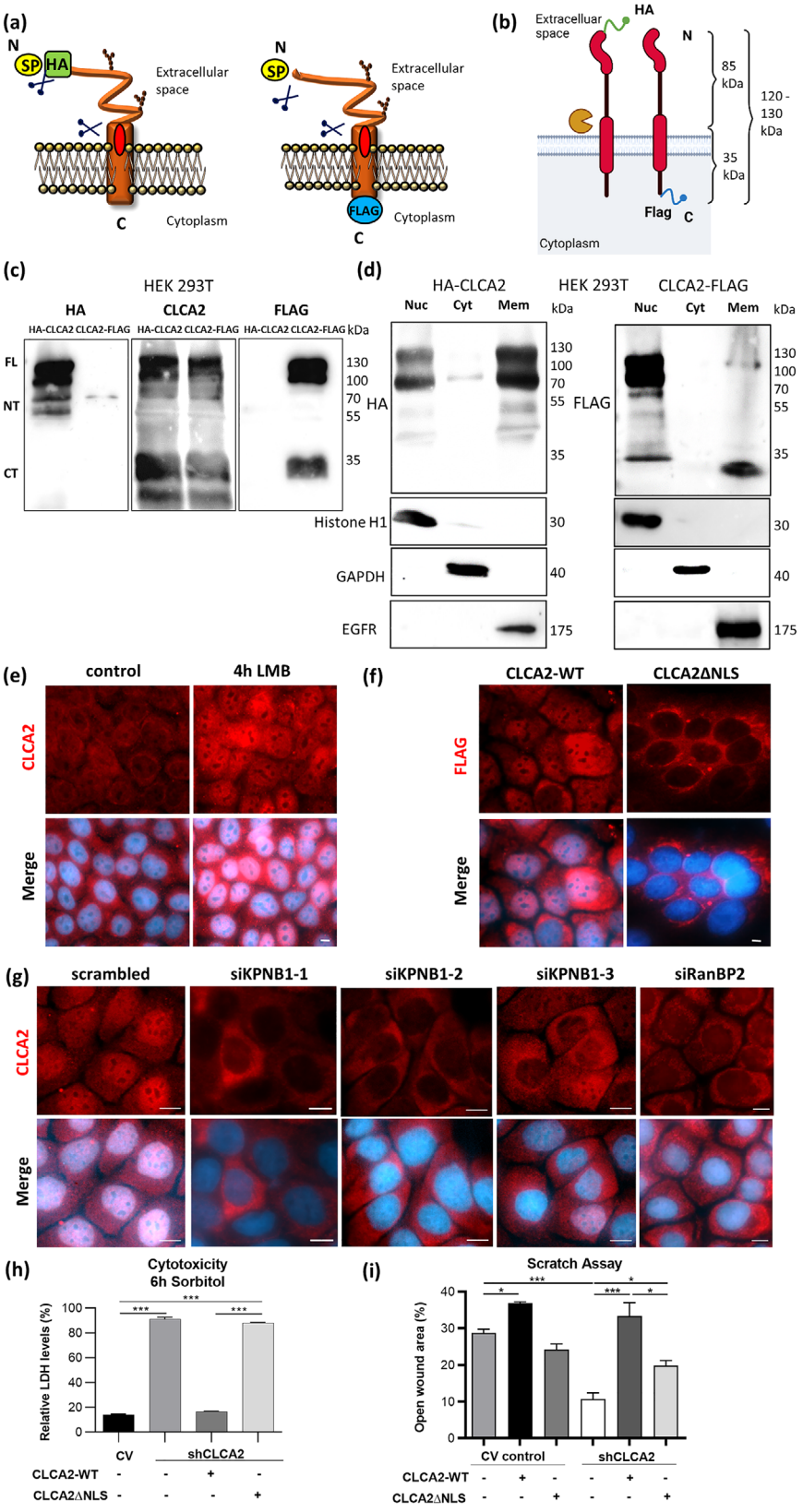

FIGURE 1 CLCA2 localizes to the plasma membrane and the nucleus. (a) Scheme of HA- and FLAG-tagged CLCA2 fusion proteins. CLCA2 has an N-terminal signal peptide (SP; cleaved off in the mature protein), a long extracellular N-terminal and a short intracellular C-terminal domain. It is glycosylated (brown trees) and can be self-cleaved into a secreted 85 kDa and a 35 kDa transmembrane fragment. The cleavage site is indicated by scissors. The epitope that is recognized by the CLCA2 antibody used in this study and present in the full-length (FL) protein and the 35 kDa fragment is indicated by a red oval. (b) Scheme displaying full-length CLCA2 and its N-terminal and C-terminal cleavage products, including their molecular weight according to Western blot analysis of keratinocyte lysates. (c, d) Western blot analysis of total (c), cytoplasmic, nuclear and membrane lysates (d) of HEK 293T cells, which had been transiently transfected with HA-CLCA2 or FLAG-CLCA2 expression vectors, using HA, FLAG or CLCA2 antibodies. Histone H1 (nuclear protein), glyceraldehyde-3-phosphate dehydrogenase (GAPDH; cytoplasmic protein) and EGFR (membrane protein) served as controls for efficient cell fractionation. FL: full-length, NT: N-terminal and CT: C-terminal fragment of CLCA2. (e) Representative CLCA2 immunofluorescence stainings (red) of HaCaT keratinocytes treated with 10 ng/mL leptomycin B (LMB) or vehicle for 4 h. Nuclei were counterstained with Hoechst (blue). (f) Representative FLAG immunofluorescence stainings (red) of HaCaT keratinocytes transiently transfected with expression vectors encoding CLCA2-WT-FLAG or CLCA2-ΔNLS-FLAG, and treated for 1 h with LMB; nuclei were counterstained with Hoechst (blue). (g) Representative CLCA2 immunofluorescence stainings (red) of HaCaT keratinocytes transfected with siRNAs against importin β1 (siKPNB1-1, siKPNB1-2 or siKPNB1-3), RanBP2 or scrambled siRNA for 48 h. Nuclei were counterstained with Hoechst (blue). (h) Relative lactate dehydrogenase (LDH) levels in the supernatant of HaCaT cells, which had been stably transduced with CLCA2 shRNA or CV lentiviruses and transiently transfected with expression vectors encoding CLCA2-WT-FLAG, CLCA2-ΔNLS-FLAG or CV (see scheme in Figure S1h) and treated with 300 mM sorbitol for 6 h ($N = 3$). (i) Area of open scratch at 28 h post wounding in confluent shCLCA2-HaCaT and CV-HaCaT keratinocytes, which had been transiently transfected with expression vectors encoding CLCA2-WT-FLAG, CLCA2-ΔNLS-FLAG or CV (see scheme in Figure S1h) and then subjected to scratch wounding. $N = 3$. Bars indicate mean ± S.E.M. $^{*}p < 0.05$, $^{***}p < 0.001$ (two-way ANOVA). Scale Bars: 10 µm. Schemes were created with BioRender.com.

presence in EVs, full-length, tagged CLCA2 as well as the 35 kDa C-terminal cleavage transmembrane product accumulated in the supernatant of CLCA2-HA-expressing HEK 293T cells over time (Figure 2a). This was not a consequence of cell lysis as demonstrated by the almost complete lack of the cytoplasmic protein lactate dehydrogenase (LDH) in the supernatant (Figure 2b). We next purified EVs by sequential ultracentrifugation (Hettich et al., 2020). EVs from non-transfected HaCaT keratinocytes indeed included full-length CLCA2 and the 35 kDa cleavage product in addition to the EV markers CD63, CD9, TSG101, and caveolin-1, but they were negative for the ER protein calreticulin (Figures 2c and S2a). Particle tracking analysis using a ZetaView Nanoparticle Tracking Analyzer with laser scattered light measuring of individual particles showed that the isolated EVs had a diameter of 50–300 nm, with a peak at 130–140 nm (Figure 2d). The concentration and size of the EVs were similar in HaCaT cells, which had been stably transduced with lentiviruses expressing CLCA2 shRNA (shCLCA2-HaCaT cells) (Seltmann et al., 2018), and in those transduced with a control viral vector (CV) without shRNA (CV-HaCaT cells) (Figures 2d and e). These EVs were labelled with DyLight 594 or 650 for further studies (see below), and TEM images of the labelled, desalted, and washed EVs displayed a field of spherical particles (Figure 2f for CV-HaCaT EVs).

RAB11 promotes exosome formation and RAB11 compartments were recently identified as conserved sites of exosome production (Fan et al., 2020; Savina et al., 2005). Therefore, we determined if CLCA2 co-localizes with RAB11. For this purpose, we transfected HaCaT cells with a plasmid encoding fluorescence-tagged RAB5 and RAB11 (Kriz et al., 2010), and stained them with an antibody against CLCA2. Co-localization of CLCA2 with both proteins was found, in particular with RAB11 (Figure S2b), further indicating that CLCA2 is incorporated into EVs.

To determine if EVs containing CLCA2 can be taken up by other cells, we exposed HEK 293T cells to EVs released by shCLCA2-HaCaT or CV-HaCaT control cells (Seltmann et al., 2018). As an additional negative control, EVs produced by non-transfected HEK 293T cells were used. Both full-length CLCA2 and the 35 kDa cleavage product were detected in the nuclear lysate of HEK 293T cells incubated with EVs from HaCaT-CV cells (Figure 2g), and their levels increased over time (Figure S2c). Nuclear CLCA2 was much less abundant when HEK 293T cells were treated with EVs from shCLCA2-HaCaT cells (Figure 2g). As expected, nuclear CLCA2 was not detected in HEK 293T cells incubated with EVs from other HEK 293T cells (Figure 2g). We next treated purified EVs from HaCaT cells with DyLight 650, which covalently labels lysine residues of membrane proteins, thereby allowing their detection by fluorescence microscopy. HaCaT cells were then incubated with the labelled, desalted, and washed EVs and analysed by confocal microscopy. DyLight 650-labelled EV membrane proteins were not only present in the cytoplasm, but also in the nucleus of the treated cells, where they co-localized with CLCA2 (Figures 2h and S2d for negative control). To visualize the uptake in greater detail, Z-stacked confocal images were displayed in three dimensions in X-Z direction (Figure 3a). For visualization, the nuclear surface was rendered using Imaris 9.5 software, and DyLight 650-labelled EV proteins (green) and immunostained CLCA2 (red) were displayed as spots using spot detection and surface function (Figures 3a and S2e). 3D modelling of confocal images revealed localization of DyLight 650-labelled EV proteins and CLCA2 at the nuclear membrane and in the nucleoplasm (Figure 3a), as well as at the Golgi apparatus as shown by co-staining with giantin (Figure S2f). To verify that HaCaT EVs enter the nucleus, we co-labelled isolated EVs with Dy-Light and with the cell permeable dye CellTrace, which is cleaved by intracellular esterases to a yield a fluorescent compound covalently bound to intracellular amines. When HaCaT cells were incubated with these double-labelled EVs, we found them inside and outside of the nucleus (Figure 3b), suggesting that EVs are at least partially intact after their nuclear uptake. Furthermore, in cells exposed to EVs that were only labelled with CellTrace, we also observed co-localization of CLCA2 and the labelled EV proteins in the nucleus, in particular at the nuclear membrane (Figure 3c). This finding strongly suggests that the labelling of membrane proteins with Dy-Light and the resulting EV surface modification does not affect the uptake and nuclear transport of EVs. Finally, we found that entry of EVs into the nucleus is not specific to keratinocytes, because DyLightTM 650-labelled EVs were also taken up by human primary fibroblasts and localized to the nucleus (Figure S2g). Upon inhibition of vesicular transport between ER and Golgi in HaCaT keratinocytes using brefeldin A, CLCA2 accumulated in the ER as expected for a transmembrane protein, but it was still detectable in the nucleus (Figure 3d). siRNA-mediated knock-down of importin β1 (*KPNB1*) and RanBP2 reduced the nuclear uptake of EVs (Figure 3e). Together, these findings further suggest that CLCA2 is transported to the nucleus via EVs.

3.4 | Nuclear CLCA2 binds and activates β-catenin in keratinocytes

To unravel the function of CLCA2 in the nucleus, we first determined if its previously identified binding partner β-catenin associates with CLCA2 not only at the cell membrane, but also in the nucleus. The interaction of β-catenin and CLCA2 in transfected HEK 293T cells, which had been observed with total lysates (Ramena et al., 2016), was confirmed by co-immunoprecipitation (IP) of both proteins from total lysates of HEK 293T cells expressing tagged CLCA2 fusion proteins (Figure 4a). In addition, the endogenous proteins interacted in HaCaT keratinocytes (Figure 4b). As expected, the amounts of β-catenin were reduced in the immunoprecipitate of shCLCA2 HaCaT cells (Figure 4b). The CLCA2-β-catenin interaction in HaCaT cells was verified using proximity ligation assay (PLA). Some PLA signals were also detected in the nucleus, suggesting that both proteins can also interact in this compartment (Figure 4c). This was confirmed by co-IP using nuclear lysates of transfected HEK 293T cells (Figure 4d). The nuclear interaction is of functional relevance, since overexpression of CLCA2-WT, but not of CLCA2-ΔNLS in

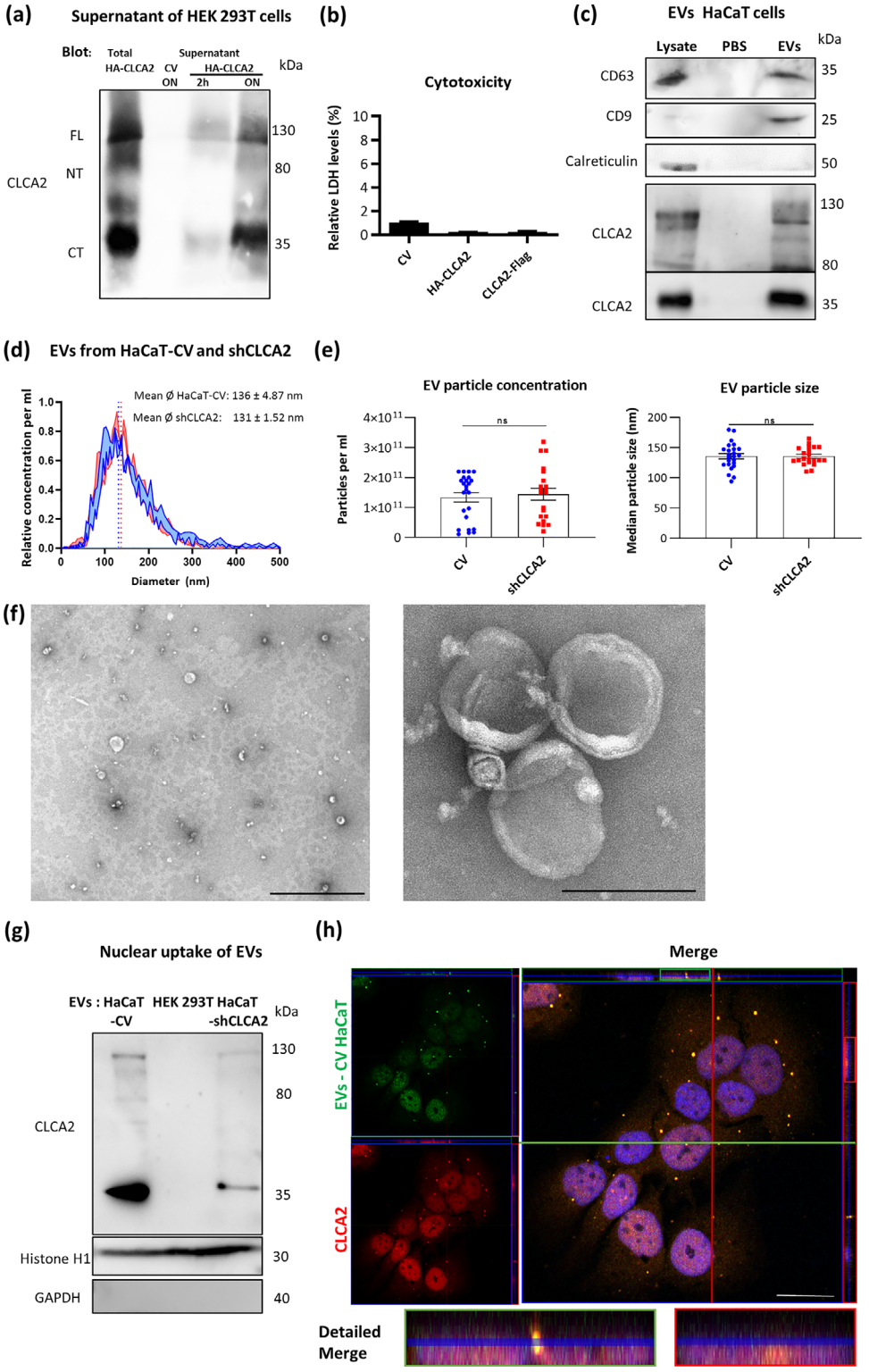

FIGURE 2 CLCA2 is present in EVs. (a) Western blot analysis of total lysates and acetone-precipitated supernatant of HEK 293T cells, which had been transiently transfected with CV or with an HA-CLCA2 expression vector, using a CLCA2 antibody. Supernatants were obtained after a 2 h or overnight (ON) incubation in serum-free medium. (b) LDH levels in the supernatant of transfected cells (see (a)) shown as percentage of the value obtained for the total cell lysate. Bars indicate mean ± SEM. $N = 3$. (c) Western blot analysis of EVs from HaCaT keratinocytes for CLCA2, the EV markers CD63 and CD9 (positive controls) and the ER marker calreticulin (negative control). (d) Particle tracking analysis of EVs isolated from CV- and shCLCA2-HaCaT cells, measured on the ZetaView Nanoparticle Tracking Analyzer in triplicates. Size distribution of the particles is shown. (e) Concentration and size of EVs isolated from the conditioned medium of shCLCA2-HaCaT or CV-HaCaT keratinocytes, measured using the ZetaView Nanoparticle Tracking Analyzer. $N = 21–24$. (f) Representative TEM images of DyLight 594 EVs from CV-HaCaT cells. Scale bars: 1000 nm (left) and 200 nm (right). (g) Western blot analysis of nuclear

(Continues)

FIGURE 2 (Continued)
lysates from HEK 293T cells, which do not express CLCA2, after incubation of the cells with EVs isolated from supernatants of shCLCA2-HaCaT or CV-HaCaT cells or with EVs from HEK 293T cells. The membrane was probed with antibodies against CLCA2, histone H1 and GAPDH. (h) Representative confocal image of HaCaT cells incubated with purified, DyLight 650-labelled EVs (green) from HaCaT cells, combined with immunofluorescence staining for CLCA2 (red) and counterstaining of nuclei with Hoechst (blue). Z-projection in the X–Z direction is shown on the top of the merge panel; side Z-projection in the Y–Z direction is shown in the right panel. Blue lines indicate the Z-depth of the 3.20 μm optical slice. The green and red lines indicate the orthogonal planes of the X–Z and Y–Z projection, respectively. The detailed merge displays provide zoomed view of Z-projections. Scale bar: 10 μm.

HaCaT cells (Seltmann et al., 2018) enhanced the levels of active (non-phosphorylated), but not of total β-catenin (Figures 4e and S1g for CLCA2 expression levels). Furthermore, knock-down of CLCA2 reduced the levels of active β-catenin in the nucleus of HaCaT cells, while CLCA2 overexpression had the opposite effect (Figure 4f). At the plasma membrane, knock-down of CLCA2 lead to a slight increase in active β-catenin levels, while overexpression of CLCA2 had no effect (Figure 4f).

3.5 | CLCA2 promotes β-catenin-mediated gene expression

Consistent with the positive effect of CLCA2 on the levels of active β-catenin (Figure 4e and f), siRNA-mediated knock-down of CLCA2 in HaCaT keratinocytes significantly reduced the expression of a TCF/LEF-driven luciferase reporter gene (TCF/LEF-reporter), while overexpression of CLCA2-WT, but not of CLCA2-ΔNLS, had the opposite effect (Figure 5a). As expected, knock-down of β-catenin suppressed expression of the reporter gene, while β-catenin overexpression induced a strong activation (Figure 5a). Moreover, transient overexpression of CLCA2-WT in HaCaT cells with stable shRNA-mediated CLCA2 knock-down rescued the expression of the reporter gene, while CLCA2-ΔNLS had no significant effect (Figures 5b; S1g for transfection control in parallel dishes).

siRNA-mediated CLCA2 knock-down also suppressed the expression of the Wnt target genes *AXIN2*, *MYC*, *CTGF*, *CCND1*, and *BMP4*, while CLCA2 overexpression strongly induced their expression (Figure 5c). Reduced expression of *CTNNB1, AXIN2*, *MYC*, and *CTGF* was also seen in shCLCA2 HaCaT cells. This was efficiently rescued by expression of CLCA2-WT, while CLCA2-ΔNLS had a much weaker effect (Figure S3).

To determine if components present in EVs, including CLCA2, activate the TCF/LEF reporter, shCLCA2-HaCaT or CV-HaCaT cells were incubated with EVs from CV-HaCaT or shCLCA2-HaCaT cells. Treatment of CV-HaCaT cells with EVs from CV-HaCaT cells caused a significant increase in luciferase activity, while shCLCA2 EVs had no effect (Figure 5d). Luciferase activity was strongly reduced upon CLCA2 knock-down. This was partially rescued by treatment of the knock-down cells with CV-HaCaT-derived EVs and to a significantly lesser extent with shCLCA2-HaCaT-derived EVs (Figure 5d). The potential of HaCaT EVs to activate the TCF/LEF reporter was abrogated in the presence of heparin, which inhibits EV uptake (Christianson et al., 2013), while inhibition of nuclear export by LMB promoted the positive effect of the EVs on reporter gene expression (Figure 5e).

3.6 | Nuclear CLCA2 interacts with proteins that control gene expression at different levels

To identify additional nuclear CLCA2 interactors in keratinocytes using an unbiased approach, we expressed CLCA2-FLAG in HaCaT cells and immunoprecipitated CLCA2-interacting proteins from nuclear lysates using beads coupled to FLAG antibodies or IgG control. Bound proteins were analysed by mass spectrometry (MS). Following a CRAPome analysis to exclude contaminants (Mellacheruvu et al., 2013), we further analysed proteins, which were detected as potential interactors in three independent experiments and with a SAINT probability (SP) score of > 0.95 (Figure 6a, table S1). The known interactor of CLCA2, integrin β4 (ITGB4) (Abdel-Ghany et al., 2003), was highly enriched in the nuclear IP (Figure 6a). This is consistent with the previously documented nuclear function of this integrin subunit (Liu et al., 2016). We also confirmed the interaction of CLCA2 with β-catenin, although only in 1 out of 3 experiments. However, the CLCA2-β-catenin interaction was confirmed in the same experimental setup by Western blot analysis of the immunoprecipitates (Figure S4a). Interestingly, some of the putative interactors identified by MS had previously been shown to be associated with Wnt signalling, such as cell cycle and apoptosis regulator (CCAR1), a co-activator of nuclear β-catenin (Ou et al., 2009). Interaction of CLCA2 with CCAR1 was confirmed by co-IP using nuclear lysates (Figure S4b). Additional putative binding partners with a previously demonstrated role in Wnt signalling are TRIM29 and nucleolar complex protein 14 (NOP14), which activated the Wnt-β-catenin pathway in cervical or colorectal cancer cells (Sun et al., 2019; Xu et al., 2016; Zhu et al., 2021).

Gene Ontology (GO) cellular component analysis revealed that the putative CLCA2 binding partners include a large number of proteins localized in specific nuclear compartments (Figure 6b). Many of these interactors are involved in RNA processing (including splicing), gene expression and ribonucleoprotein complex biogenesis as shown by GO biological process analysis (Figures 6c and S4c for the individual proteins). Importantly, various proteins with known location in the inner nuclear mem-

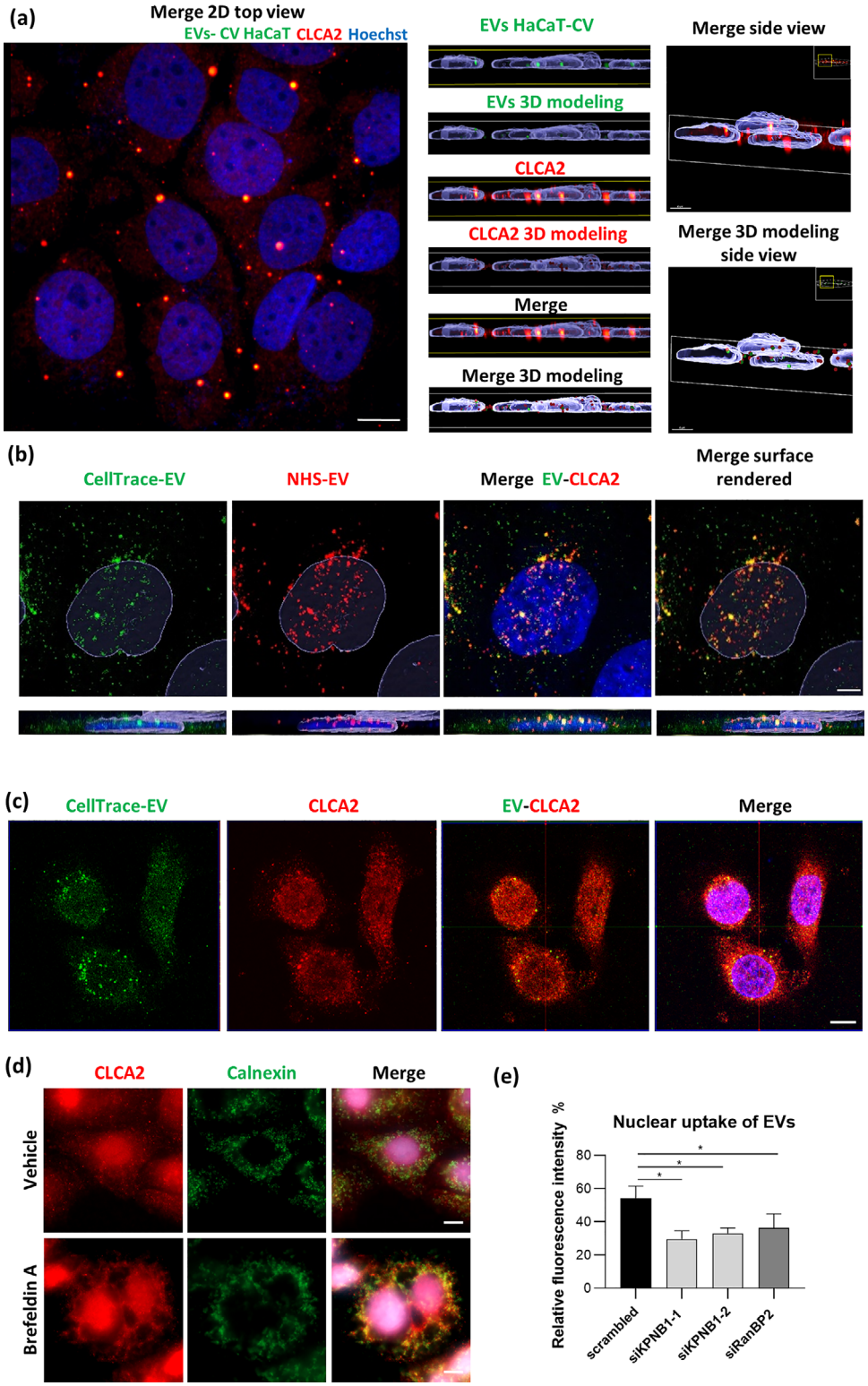

FIGURE 3 CLCA2 can be transported to the nucleus by EVs. (a) 3D modelling of representative confocal images of HaCaT cells, which had been incubated with DyLight 650-labelled EVs (green) from HaCaT cells and immunostained for CLCA2 (red). Nuclei were counterstained with Hoechst (blue). Top view and clipping plane of Z-projection in X-Z direction in front (middle) and shifted in-side view (right) are displayed. For visualization of the nucleus, the surface was rendered and combined with fluorescence data. For 3D modelling images, additionally to the nucleus, EVs and CLCA2 were rendered as spots with focus on particle size and overlaid. Note the co-localization of fluorescence labelled EV proteins and CLCA2 inside and outside of the nucleus. Scale bar: 5 µm. (b) Representative confocal image of HaCaT cells incubated with EVs, which had been co-stained with CellTrace (green) and DyLight 594 (red). Nuclei were counterstained with Hoechst (blue). For 3D modelling, Hoechst staining was used to render the surface of the nucleus (Imaris software). For visualization, clipping planes were inserted in X-Z direction shifted in front (bottom). Scale bar: 5 µm. (c) Representative confocal images of HaCaT keratinocytes, which had

(Continues)

FIGURE 3 (Continued)
been incubated with CellTrace-labelled EVs (green), combined with immunofluorescence staining for CLCA2 (red) and counterstaining of nuclei with Hoechst (blue). CLCA2 and labelled EV proteins co-localize inside and outside of the nucleus. Scale bar: 10 μm. (d) Representative immunofluorescence stainings of HaCaT keratinocytes treated with brefeldin A or vehicle overnight, using CLCA2 (red) and calnexin (green) antibodies; nuclei were counterstained with Hoechst (blue). CLCA2 that is present in the ER appears yellow. Scale bar: 10 μm. (e) Relative fluorescence intensity of HaCaT keratinocytes incubated with DyLight 650-labelled EVs and counterstained with Hoechst. Quantification of EV uptake was performed by analysing DyLight 650 fluorescence intensity relative to Hoechst fluorescence.

brane as well as components of the nuclear transport machinery were identified as putative CLCA2 binding partners (Figures S4d and e), further suggesting an active transport of CLCA2 into the nucleus.

3.7 | RBM3 is a CLCA2 binding partner, which also activates Wnt signalling

A particularly high interaction probability was observed for RBM3, which was identified in all three MS analyses (Figure 6a). RBM3 had previously been shown to regulate Wnt signalling in colorectal cancer cells by suppression of glycogen synthase kinase (GSK) 3β activity, which in turn stabilizes β-catenin (Venugopal et al., 2016). It is also involved in the regulation of gene/protein expression at multiple levels, including promotion of mRNA stability, splicing and protein translation (Dresios et al., 2005; Liu et al., 2022; Wellmann et al., 2010; Zeng et al., 2013). Interaction of CLCA2 with RBM3 was confirmed by co-IP of nuclear lysates (Figure 6d). This interaction seems to stabilize RMB3, since siRNA-mediated knock-down of CLCA2 in HaCaT cells strongly reduced the levels of RBM3 protein (Figure 6e). Vice versa, siRNA-mediated knock-down of RBM3 reduced the levels of CLCA2 and also of active β-catenin in HaCaT cells (Figure 6f). Consistently, RBM3 knock-down reduced the expression of a TCF/LEF-driven luciferase reporter to a similar extent as CLCA2 knock-down, and a mild further decline was observed upon knock-down of both proteins (Figures 6g and S5a for knock-down efficiency). Expression of *CTNNB1* and the Wnt target genes *AXIN2* and *MYC* was also reduced following knock-down of either RBM3 or CLCA2 (Figure 6h). Interestingly, knock-down of RBM3 also reduced CLCA2 mRNA levels (Figure 6h), suggesting that the reduction of CLCA2 protein levels by RBM3 knock-down (Figure 6f) is at least partially mediated at the RNA level. By contrast, CLCA2 knock-down did not significantly reduce the mRNA levels of RBM3 (Figure 6h).

3.8 | RBM3 overexpression partially rescues the low expression of Wnt target genes in CLCA2 knock-down cells

The data obtained so far strongly suggest that the CLCA2 binding partner RMB3 is required for at least some of the biological activities of nuclear CLCA2. To further test this possibility, we performed gain-of-function rescue experiments. Overexpression of RBM3 in wild-type HaCaT cells strongly induced the expression of the Wnt target genes *AXIN2* and *MYC*. Most importantly, the reduced expression of these genes in CLCA2 knock-down cells was partially rescued by overexpression of RBM3 (Figure 7a). Consistent with these results, overexpression of RBM3 or CLCA2 increased the TCF/LEF-dependent luciferase activity in CV-HaCaT cells and partially rescued the low luciferase activity in shCLCA2-HaCaT cells (Figure 7b). This may result at least in part from the increase in CLCA2 levels upon overexpression of CLCA2 or RBM3 in cells with CLCA2 knock-down (Figure S5b). There was only a mild, but non-significant additive effect when both CLCA2 and RBM3 were overexpressed (Figure 7b). By contrast, overexpression of CLCA2 in RBM3 knock-down keratinocytes did not increase Wnt target gene expression (Figure 7c) or TCF/LEF-dependent luciferase activity (Figure 7d), suggesting that RBM3 is required for CLCA2-mediated TCF/LEF promoter activation and expression of Wnt targets genes.

3.9 | CLCA2 and RBM3 collaborate to control keratinocyte migration and survival

Finally, we determined if RBM3 also affects keratinocyte migration and survival and if its overexpression rescues the effect of CLCA2 knock-down on these activities. Indeed, siRNA-mediated knock-down of RBM3 also increased migration of keratinocytes (Figure 7e). In addition, siRNA-mediated knock-down of either CLCA2 or RBM3 reduced the metabolic activity of keratinocytes subjected to the hyperosmotic stress-inducing compound sorbitol, indicating reduced survival (Figure 7f). This was verified in an LDH assay, where knock-down of either CLCA2 or RBM3 resulted in enhanced LDH levels in the culture supernatant of sorbitol-treated cells, which reflects cell lysis (Figure 7g).

Overexpression of CLCA2-WT or RBM3-WT in shRNA-mediated CLCA2 knock-down keratinocytes abrogated the enhanced migration of these cells (Figure 7h) and strongly reduced the extent of cell death upon sorbitol treatment (Figure 7i), further demonstrating that RBM3 is required for important biological activities of CLCA2.

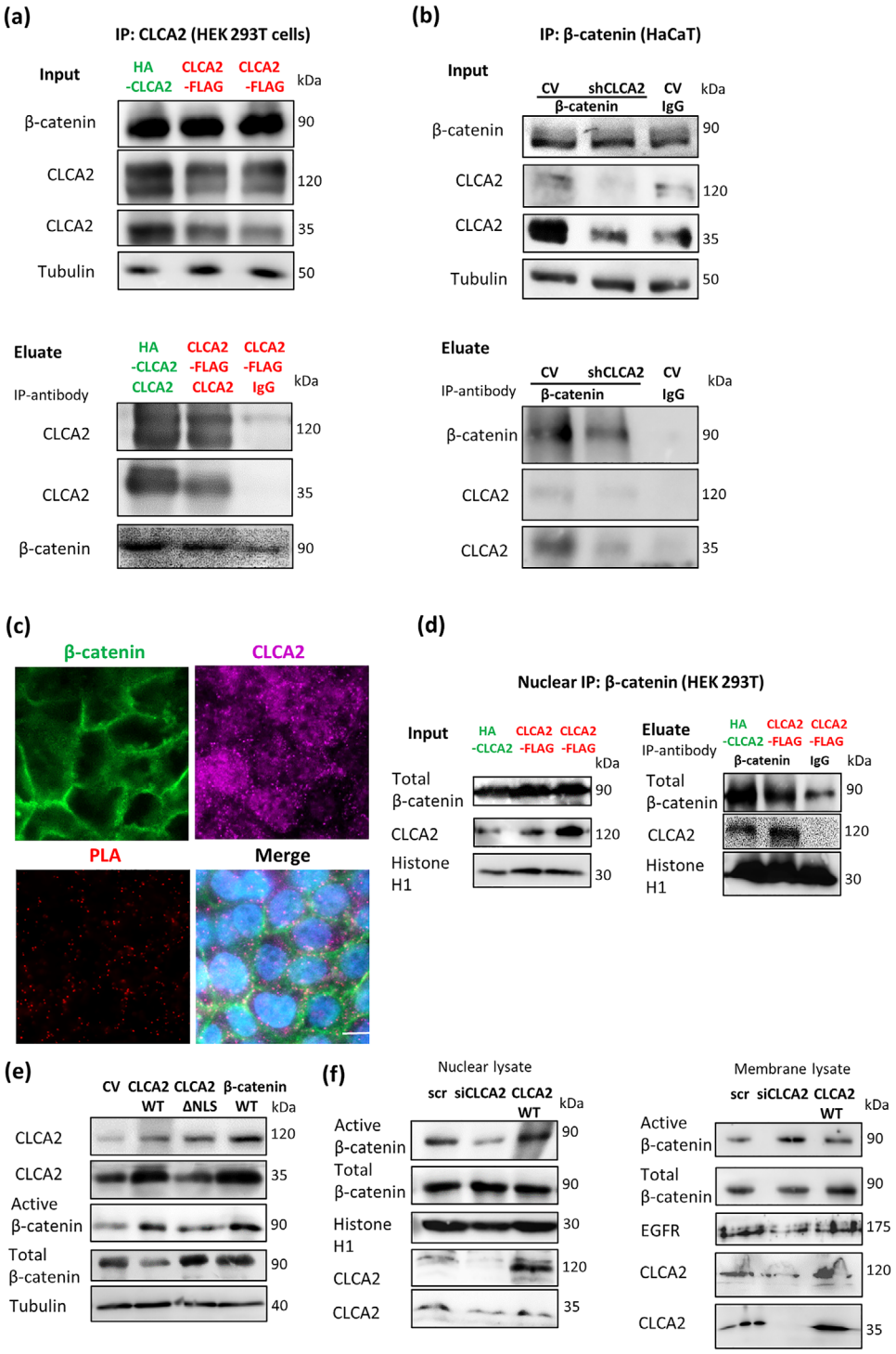

FIGURE 4 Co-localization of CLCA2 and β-catenin and their nuclear interaction in keratinocytes. (a) Western blot analysis of lysates (input; upper panel) and immunoprecipitates (eluate; lower panel) of HEK 293T cells, which had been transfected with HA-CLCA2 (left lanes) or FLAG-CLCA2 (middle and right lanes) expression vectors, using antibodies against CLCA2 and β-catenin. Precipitation was performed with a CLCA2 antibody (Co-IP) or IgG control. Tubulin was used as a loading control for the input. (b) Western blot analysis of lysates (input) or immunoprecipitates (eluate; lower panel) of HaCaT keratinocytes, which had been stably transduced with lentiviruses expressing CLCA2 shRNA or of CV cells, using antibodies against β-catenin and CLCA2. Precipitation was performed with a β-catenin antibody or IgG control. (c) Representative confocal images of HaCaT cells analysed by in situ proximity ligation assay (PLA; red) using antibodies against β-catenin (green) and CLCA2 (pink). Maximum intensity projections of confocal z-stacks were performed to observe the maximum amount of PLA puncta. Scale bars: 10 μm. (d) Western blot analysis (left panel; input) or immunoprecipitates (right panel; eluate) of nuclear lysates from HEK 293T cells, which had been transiently transfected with HA-CLCA2 or FLAG-CLCA2 expression vectors for 72 h, using antibodies against β-catenin, CLCA2 and histone H1. Precipitation was performed with a β-catenin antibody or IgG control. (e) Western blot analysis of total lysates of HaCaT cells, which had been transiently transfected with FLAG-CLCA2-WT, FLAG-CLCA2-ΔNLS or β-catenin expression vectors or CV, using antibodies against CLCA2, active and total β-catenin, and tubulin. (f) Western blot analysis of nuclear and membrane lysates from HaCaT cells, which had been transiently transfected with CLCA2 or scrambled (scr) siRNAs or with an HA-CLCA2 expression vector (CLCA2-WT) for 48 h, using antibodies against active and total β-catenin, CLCA2, histone H1 and EGFR.

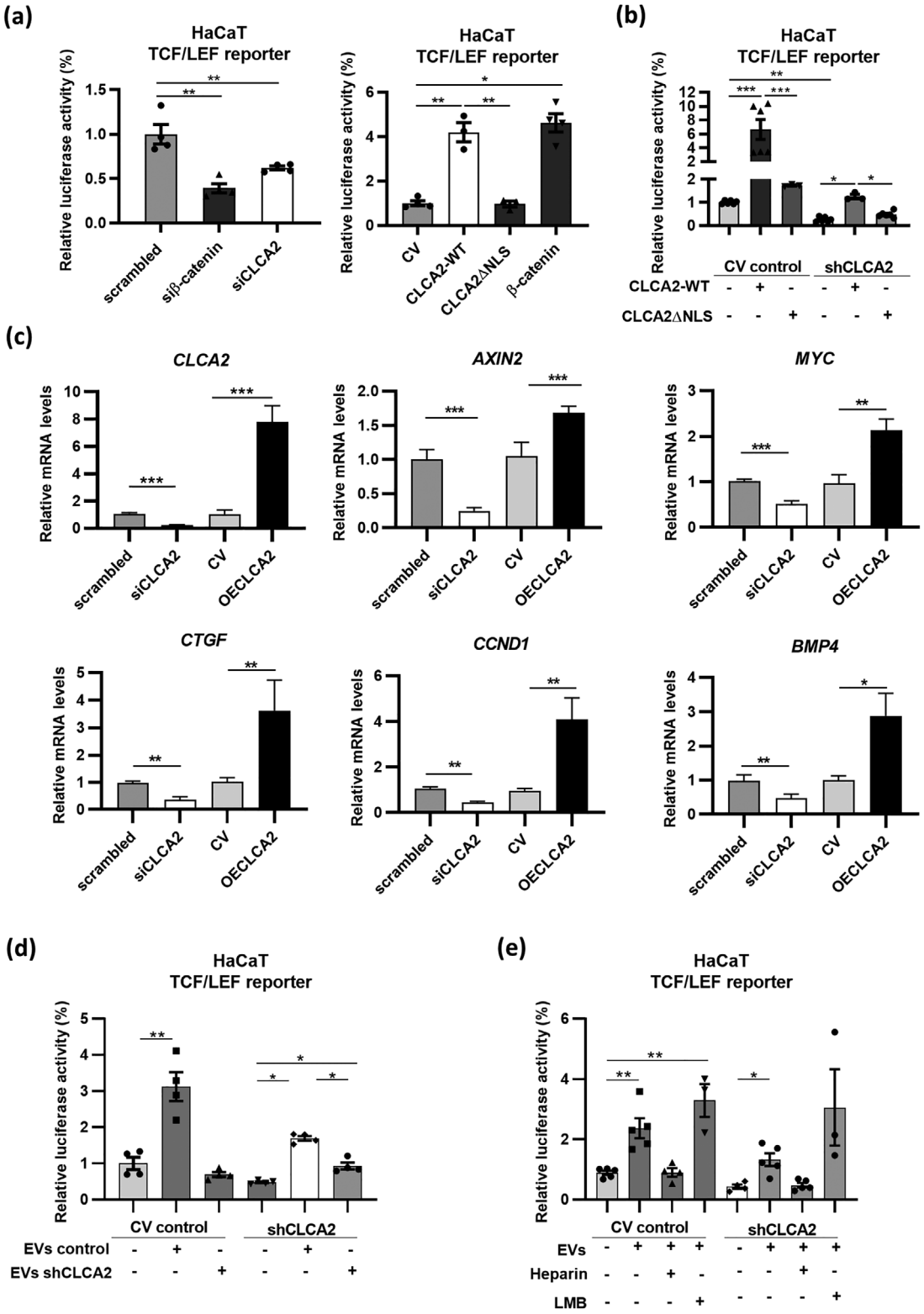

FIGURE 5 CLCA2 regulates expression of WNT target genes. (a) Ratio of Firefly versus Renilla luciferase activities in HaCaT cells, which had been transfected with CLCA2 (siCLCA2), β-catenin (siβ-catenin) or scrambled siRNAs, with FLAG-CLCA2-WT, FLAG-CLCA2-ΔNLS or β-catenin expression vectors or with CV, as well as with a TCF/LEF firefly luciferase reporter construct and a Renilla luciferase expression vector for normalization (see scheme in Figure S1h). Luciferase activities were determined 72 h after plasmid DNA transfection. Mean relative luciferase activity in cells transfected with scrambled siRNA was set to 1. $N = 4$. (b) Ratio of Firefly versus Renilla luciferase activities in shCLCA2-HaCaT or CV-HaCaT cells 72 h after transient transfection with FLAG-CLCA2-WT or FLAG-CLCA2-ΔNLS expression vectors or CV together with a TCF/LEF firefly luciferase reporter construct and a Renilla luciferase expression vector. $N = 3$–5. Mean relative luciferase activity in CV control cells was set to 1. (c) qRT-PCR analysis for *CLCA2* and the Wnt target genes *AXIN2, MYC, CTGF, CCND1*, and *BMP4* relative to *RPL27* using RNA from HaCaT cells isolated 72 h after transient transfection with CLCA2 or scrambled siRNAs or

(Continues)

FIGURE 5 (Continued)

with an HA-CLCA2 expression vector (Overexpression CLCA2; OECLCA2). Mean expression levels in cells transfected with scrambled siRNA were set to 1. $N = 5–6$. (d) Ratio of Firefly versus Renilla luciferase activities in shCLCA2-HaCaT or CV-HaCaT cells, which had been transiently transfected with a TCF/LEF firefly luciferase reporter construct and a Renilla luciferase expression vector and incubated overnight with or without EVs from CV-HaCaT or shCLCA2-HaCaT cells. Luciferase activities were determined 72 h after transfection. $N = 4$. Mean relative luciferase activity in CV control cells was set to 1. (e) Ratio of Firefly versus Renilla luciferase activities in shCLCA2-HaCaT or CV-HaCaT cells, which had been transfected as described in (d) and were pre-treated with heparin, leptomycin B (LMB) or vehicle, followed by overnight incubation with or without EVs from HaCaT cells. Mean relative luciferase activity in untreated, CV-transduced cells was set to 1. $N = 3–5$. Graphs show mean ± S.E.M. $^{*}p \leq 0.05$; $^{**}p \leq 0.01$, $^{***}p \leq 0.001$ (two-way ANOVA).

3.10 | CLCA2 and RBM3 co-localize in the epidermis of human foreskin

Finally, we determined the potential *in vivo* relevance of our findings by analyzing the expression of CLCA2 and RBM3 in human foreskin. Immunofluorescence staining showed co-localization of CLCA2 and RBM3 in the basal and suprabasal layers of the epidermis (Figures 8a and S6). Importantly, CLCA2 was also detected in the nuclei of these cells *in vivo* (Figure 8a). The interaction between CLCA2 and RBM3 *in vivo* was confirmed using PLA, whereby the PLA signals were mainly detected in the nucleus (Figure 8b). These results suggest that a CLCA2/RBM3 complex also regulates gene expression in keratinocyte nuclei *in vivo*.

4 | DISCUSSION

We made the surprising discovery that CLCA2, which is known for its functions as a transmembrane protein, localizes to the nucleus of keratinocytes where it mediates important cellular activities. Our results strongly suggest that the nuclear transport of CLCA2 is mediated at least in part via EVs: (i) CLCA2 was detected in EVs secreted by keratinocytes, (ii) it accumulated in the nucleus of HEK 293T cells upon treatment with CLCA2-containing keratinocyte EVs, which required importin β1 and RanBP2, and (iii) treatment of keratinocytes with CLCA2-containing EVs promoted TCF/LEF reporter gene expression, which was blocked by heparin and enhanced by LMB-mediated inhibition of nuclear export.

While uptake of proteins into the cytoplasm via EVs has been reported for several cell types (Lo Cicero et al., 2015; Mathieu et al., 2019) and has even been shown to modulate Wnt signalling (Luga et al., 2012; Zhang et al., 2015), EV-mediated transport of membrane proteins to the nucleus is poorly investigated. A previous study showed that EV-derived biomaterial is transported to the nucleus of mesenchymal stromal cells, which involves a sub-nuclear compartment created by late endosomes and nuclear envelope invaginations, where biomaterials associated with EVs are delivered (Rappa et al., 2017). Furthermore, EGFR and androgen receptor had been shown to be transported to the nucleus via EVs (Read et al., 2017). Therefore, this poorly characterized EV-mediated transport mechanism of membrane proteins to the nucleus could be of general relevance and may even be a strategy of cells to control gene expression in neighbouring cells (Corbeil et al., 2020). The nuclear uptake of CLCA2 required its NLS as well as importin β1 (KPNB1) and RanBP2, which is consistent with a transport through nuclear pores. EVs have a diameter range of 30–500 nm (Welsh et al., 2023, 2024), and only small EVs are expected to go through the nuclear pore. It is also possible that EVs fuse with the nuclear membrane or that material is shed from EVs for nuclear translocation. Investigation of the detailed molecular mechanism underlying this trafficking process and the fate of the EVs at the nuclear membrane was beyond the scope of this study, but this should be addressed in future work. In addition, it will be interesting to determine if CLCA2 and other membrane proteins can be transported to the nucleus of other cell types *in vivo* using the EV-mediated transport mechanism discovered in this study. Potentially, specific EV subtypes may be involved, which could mediate short-range and/or long-range signalling.

Here we focused on the identification of relevant nuclear functions and binding partners of CLCA2. We showed that CLCA2 interacts with β-catenin in the nucleus, possibly at the nuclear membrane. This is of functional relevance, since the NLS located in the cytoplasmic tail of CLCA2 was required for activation of β-catenin and efficient expression of a TCF/LEF reporter gene and of endogenous Wnt target genes. It remains to be determined if a direct physical interaction of CLCA2 with β-catenin is required for this effect, and/or if it involves its binding to RBM3, CCAR1 and/or other nuclear proteins (see below). Surprisingly, CLCA2 overexpression in MCF7 breast cancer cells reduced the levels of total β-catenin and the expression of some Wnt target genes (Ramena et al., 2016), while we did not observe an effect of CLCA2 on total β-catenin levels in keratinocytes, and the amounts of active β-catenin even increased. These apparently contradictory results may reflect cell type-specific differences and/or different consequences of the interaction of both proteins at the plasma membrane versus the nucleus. Consistent with the latter possibility, we found that the nuclear localization of CLCA2 is important for the activation of β-catenin and of Wnt target gene expression. It is possible that CLCA2 is not targeted to the nucleus of MCF7 cells, for example, because of differences in EV composition or function, or that it does not interact with β-catenin in the nucleus of these cancer cells.

Our results further show that CLCA2 suppresses keratinocyte migration. This is consistent with the suppression of migration and of invasive growth of breast cancer cells by CLCA2 (Sasaki et al., 2012; Walia et al., 2012). In keratinocytes, the effect on migration also required the presence of CLCA2 in the nucleus. It may involve its positive effect on β-catenin activity, since β-

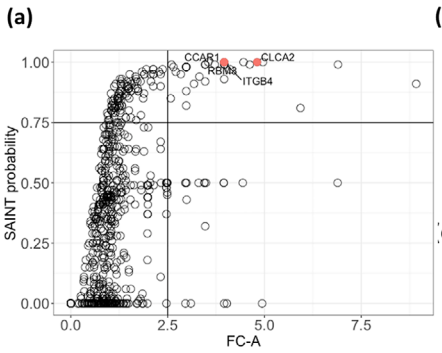

(b)

GO Cellular Component	FDR	% of input
Ribonucleoprotein complex	3.14E-11	38.64
Nucleoplasm	1.99E-09	61.36
Nuclear lumen	1.99E-09	65.91
Intracellular organelle lumen	1.05E-08	70.45
Nucleus	5.01E-08	77.27

(c)

GO Biological processes	FDR
RNA processing	2.50E-11
mRNA splicing, via spliceosome	9.32E-09
mRNA processing	2.54E-08
Gene expression	7.92E-07
Ribonucleoprotein complex biogenesis	1.15E-06

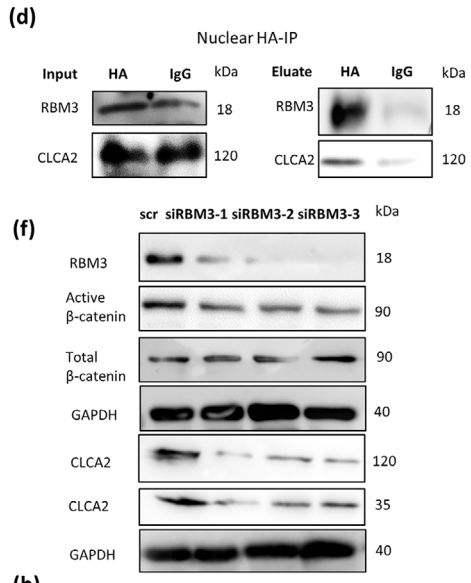

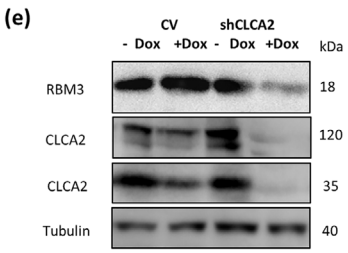

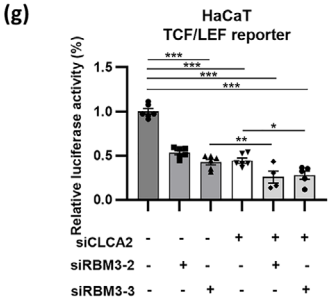

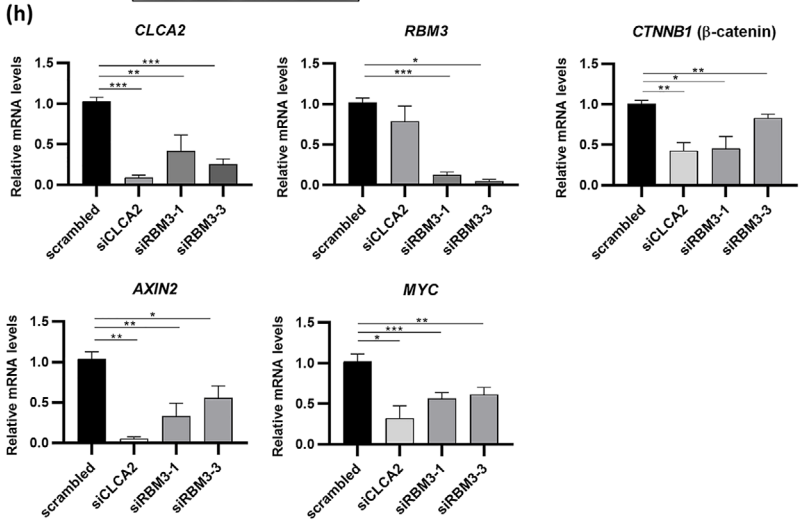

FIGURE 6 RBM3 is a nuclear CLCA2 binding partner. (a) Fold change (FC)-A and Saint probability (SP) output based on CRAPome analysis of proteins from nuclear lysates of HaCaT cells transfected with a FLAG-CLCA2 expression vector and immunoprecipitated using beads coupled to a FLAG antibody. Precipitated proteins were identified by mass spectrometry. Beads-only controls were used for comparison. Solid lines indicate FC-A > 2.50 and SP > 0.75. Interacting proteins described in the manuscript are indicated. (b) 43 putative nuclear CLCA2-FLAG binding proteins (SP > 0.95) were subjected to functional enrichment analysis using enrichR. The top 5 Gene Ontology (GO) Cellular Components with false discovery rate (FDR) and percentage of input are shown. (c) The proteins presented in (b) were subjected to functional enrichment analysis using enrichR. The top 5 GO Biological Processes with FDR are shown. (d) Western blot analysis of nuclear lysates (left panel; input) or immunoprecipitates from nuclear lysates (right panel; eluate) of HaCaT cells, which had been transfected with an HA-CLCA2 expression vector for 72 h, using antibodies against CLCA2 and RBM3. Co-IP was performed with anti-HA-coupled or IgG control beads. (e) Western blot analysis of total lysates from HaCaT cells stably transduced with shCLCA2 or CV lentiviruses and treated with doxycycline (Dox) or vehicle (DMSO) for 72 h, using antibodies against RBM3, CLCA2 and GAPDH. (f) Western blot analysis of total lysates of HaCaT cells, which had been transfected with different RBM3 siRNAs or scrambled (scr) siRNA for 48 h, using antibodies against RBM3, active and total β-catenin, CLCA2 and GAPDH. (g) Ratio of Firefly versus Renilla luciferase activities in HaCaT cells, which had been transfected with CLCA2 (siCLCA2), RBM3 (siRBM3-2 or siRBM3-3), or scr siRNAs or combinations, together with a TCF/LEF firefly luciferase reporter construct and a Renilla luciferase expression vector, 72 h after transfection. Mean relative luciferase activity in cells transfected with scr siRNA was set to 1. $N = 4$–6. (h) qRT-PCR analysis for *CLCA2, RBM3* and the Wnt target genes *CTNNBI, AXIN2* and *MYC* relative to *RPL27* using RNA from HaCaT cells, which had been transfected with CLCA2, RBM3 or scr siRNAs, 48 h after transfection. Mean expression levels in cells transfected with scr siRNA were set to 1. $N = 6$.

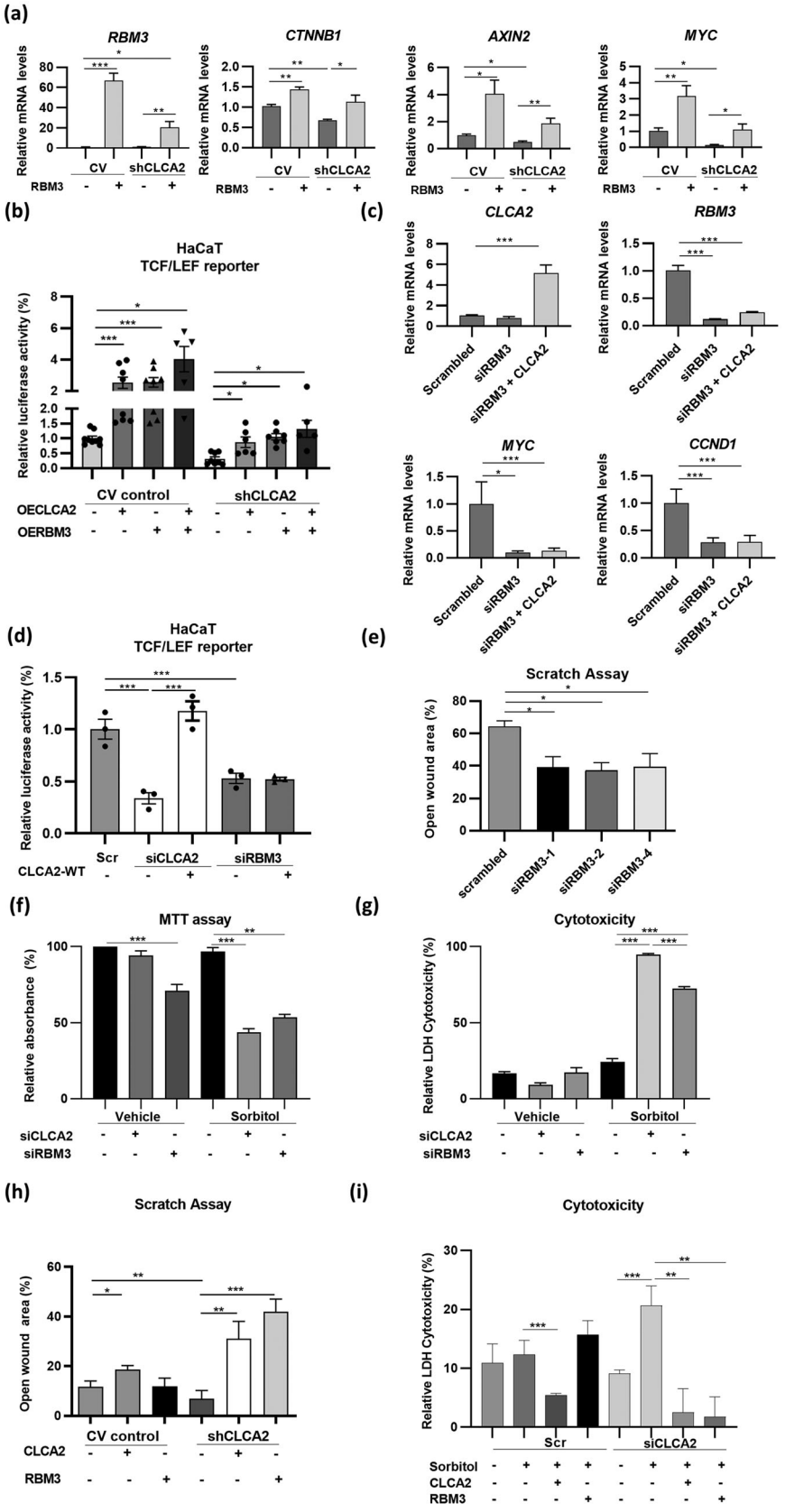

FIGURE 7 RBM3 overexpression rescues the effects of CLCA2 knock-down in keratinocytes. (a) qRT-PCR analysis for *RBM3*, *CTNNB1, AXIN2* and *MYC* relative to *RPL27* using RNA from shCLCA2-HaCaT or CV-HaCaT cells transiently transfected with an RBM3 expression vector or CV, 72 h after transfection. Mean expression levels in CV-HaCaT cells were set to 1. $N = 6$. (b) Ratio of Firefly versus Renilla luciferase activities in HaCaT cells, which had been stably transduced with shCLCA2 or CV lentiviruses and transiently transfected with HA-CLCA2 and/or RBM3 expression vectors or CV together with a TCF/LEF firefly luciferase reporter construct and a Renilla luciferase expression vector, 72 h after transfection. Mean relative luciferase activity in CV-HaCaT cells was set to 1. $N = 3$. (c) qRT-PCR analysis for *CLCA2*, *RBM3* and the Wnt target genes *MYC and CCND1* relative to *RPL27* using RNA from HaCaT cells, which had been transfected with RBM3 or scr siRNAs, and with a CLCA2 expression vector or CV (see scheme in Figure S1h). Expression levels in CV-transduced cells were set to 1. $N = 5$–8. (d) Ratio of Firefly versus Renilla luciferase activities in HaCaT cells, which had been transfected with CLCA2 (siCLCA2), RBM3 (siRBM3) or scr siRNAs and with a CLCA2 expression vector or CV, together with a TCF/LEF firefly luciferase reporter construct and a Renilla luciferase expression vector, 72 h after transfection. Mean relative luciferase activity in cells transfected with scr siRNA was set to 1. $N = 3$. (e) Percentage of open scratch at 28 h post wounding of confluent HaCaT cells, which had been transfected with different RBM3 siRNAs or scr siRNA for 48 h. $N = 3$. (f) Metabolic activity based on MTT assay in HaCaT cells, which had been transfected with CLCA2, RBM3 or scr siRNAs for 48 h and then treated with 300 mM sorbitol for 6 h. $N = 4$. Absorbance in vehicle-treated cells transfected with scr siRNA was set to 100%. (g) Relative LDH levels in the supernatants of HaCaT cells, which had been transfected with CLCA2, RBM3 or scr siRNAs for 48 h and then treated with 300 mM sorbitol for 6 h. $N = 3$–4. 100% corresponds to death of all cells. (h) Percentage of open scratch at 24 h post wounding of confluent shCLCA2-HaCaT and CV-HaCaT cells, which had been transiently transfected with expression vectors encoding CLCA2-WT-FLAG or RBM3 or CV. $N = 4$. (i) Relative LDH levels in the supernatants of HaCaT cells, which had been transfected with CLCA2 or scr siRNAs and/or CLCA2 or RBM3 expression vectors or CV and then treated with 300 mM sorbitol for 6 h $N = 3$. Graphs show mean ± SEM. $^{*}p \leq 0.05$; $^{**}p \leq 0.01$, $^{***}p \leq 0.001$ (two-way ANOVA).

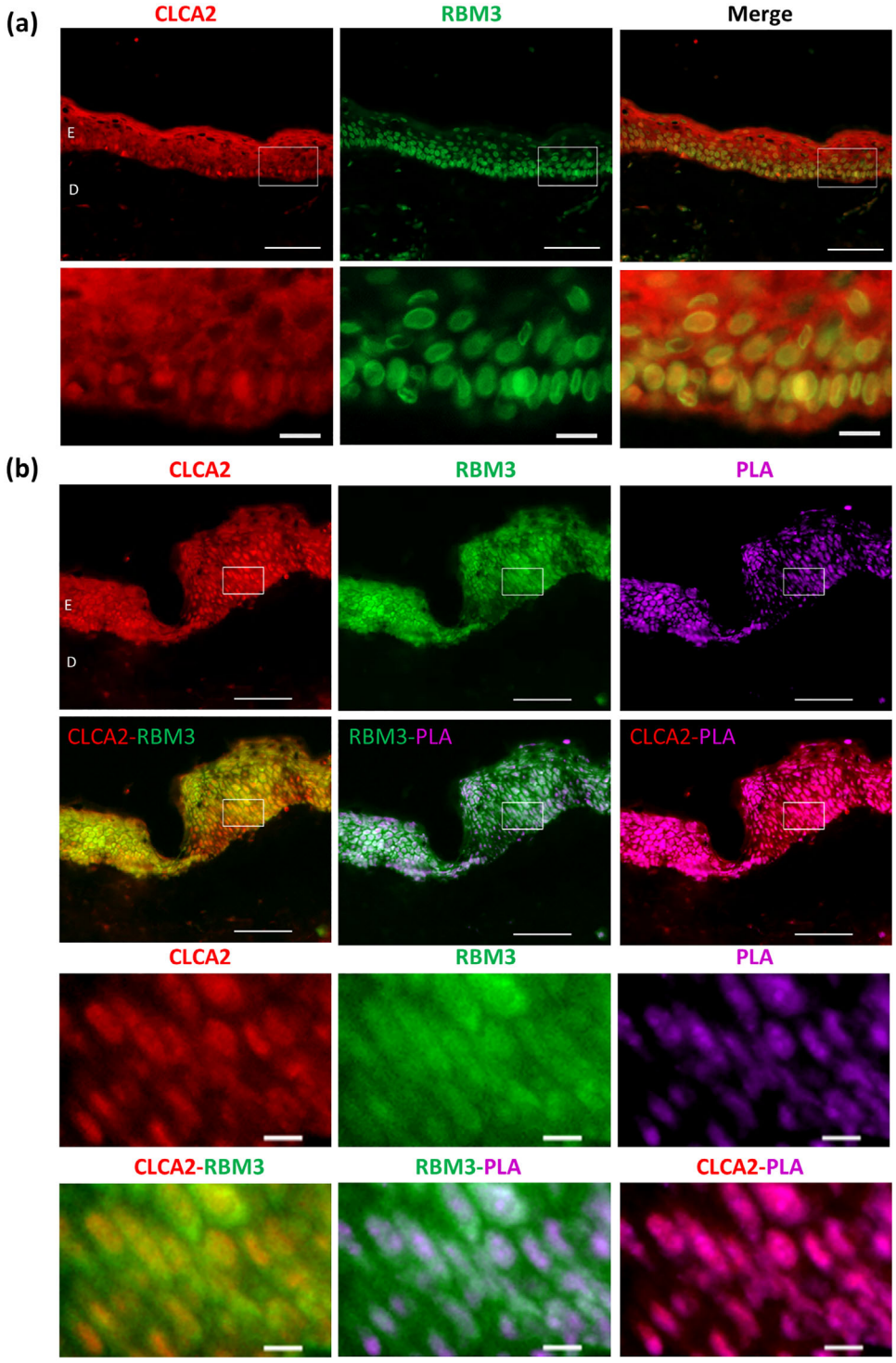

FIGURE 8 Co-localization of CLCA2 and RBM3 in the human epidermis. (a) Representative immunofluorescence stainings of sections from human foreskin with antibodies against CLCA2 (red) and RBM3 (green). Note the co-expression of CLCA2 and RBM3 in keratinocyte nuclei. The area indicated with a white box is shown at higher magnification below. Scale bars: 100 μm (overview) or 10 μm (high magnification). D: Dermis; E: Epidermis. (b) Representative confocal images of HaCaT cells analysed by in situ proximity ligation assay (PLA; purple) using antibodies against RBM3 (green) and CLCA2 (red). Note the interaction of CLCA2 and RBM3 in the nucleus (magenta). The area indicated with a white box is shown at higher magnification below. Scale bars: 100 μm (overview) or 10 μm (high magnification).

catenin activation inhibited migration of human keratinocytes in vitro, and β-catenin is present in keratinocytes at the edge of chronic ulcers, which fail to migrate (Stojadinovic et al., 2005).

The increased migration of keratinocytes that we observed upon knock-down of CLCA2 was reversed by transient overexpression of the wild-type protein, but only partially by overexpression of the ΔNLS mutant. Although CLCA2-ΔNLS showed proper expression and localization at the plasma membrane as well as binding to E-cadherin and β-catenin, we cannot fully exclude the possibility that this mutation also affects CLCA2 activities at the plasma membrane, for example, through alterations in protein folding and/or in the interaction with other proteins. Independent of this open question, the identification of binding partners of wild-type CLCA2, which are involved in RNA processing, gene expression and ribonucleoprotein complex biogenesis, suggests important additional functions of CLCA2 in the nucleus. Of particular interest in this context is its binding to RBM3, which we identified in this study. Similar to CLCA2, RBM3 had been detected in different cellular compartments, including the nucleus (Zhu et al., 2016). It was also found in EVs released from several cell lines (Kugeratski et al., 2021), suggesting that both CLCA2 and RMB3 may be transported to the nucleus via EVs, which could support their interaction.

Knock-down of RBM3 affected Wnt signalling in keratinocytes to a similar extent as knock-down of CLCA2. This is in line with the previously demonstrated regulation of Wnt signalling by RBM3 through suppression of GSK3β activity, which in turn stabilized β-catenin in colorectal cancer cells (Venugopal et al., 2016). While we do not know if this mechanism is also important in keratinocytes, RBM3 overexpression rescued the defect in the expression of the TCF/LEF reporter in keratinocytes with CLCA2 knock-down. These data strongly suggest that efficient Wnt target gene expression requires CLCA2 and its binding partner RBM3. Importantly, the enhanced migration of CLCA2 knock-down keratinocytes and their reduced survival under hyperosmotic stress conditions were also reverted by RBM3 overexpression. This may involve the positive regulation of CLCA2 expression by RBM3, for example, through binding of RBM3 to CLCA2 transcripts, and/or a CLCA2-independent downstream activity. Studies with *CLCA2* knockout cells, in which RBM3 can no longer promote CLCA2 expression, will be required to distinguish between these possibilities. However, our preliminary data suggest that *CLCA2* knockout keratinocytes already show reduced survival under non-challenged conditions. This underlines the important role of CLCA2 as a stress-protective protein, but it will complicate any rescue experiments with these cells.

Finally, our work revealed that knock-down of either CLCA2 or RBM3 promoted keratinocyte migration and that both proteins are required for keratinocyte survival in response to hyperosmotic stress ((Seltmann et al., 2018) and this study). This may involve the interaction of both proteins, as suggested by the importance of the nuclear localization of CLCA2 for both activities. Therefore, our new and previous data (Seltmann et al., 2018) show that CLCA2 promotes the survival of keratinocytes exposed to hyperosmotic stress through the regulation of yet unknown genes, RNAs or proteins in the nucleus and also ensures epidermal integrity under these conditions through promotion of cell-cell adhesion (Seltmann et al., 2018), an activity that requires its presence at the cell membrane. Interestingly, RBM3 also conferred resistance of different cell types to various other stressors, including serum withdrawal, ER stress and cold exposure and protected cells from apoptosis (Hu et al., 2022; Zhu et al., 2016). It remains to be determined if these cytoprotective activities also involve its binding partner CLCA2. Independent of this open question, our work suggests that the CLCA2-RBM3 partnership is also relevant in human skin *in vivo*, as both proteins co-localize in the nuclei of basal and suprabasal keratinocytes. Most importantly, we previously showed that CLCA2 is strongly expressed in the epidermis of Atopic Dermatitis patients, where it likely protects keratinocytes from hyperosmotic stress that occurs as a consequence of the impaired epidermal barrier and resulting transepidermal water loss (Seltmann et al., 2018). In the future, it will be of interest to determine if this function requires RBM3 and if CLCA2 and RBM3 are targeted to the keratinocyte nucleus in the skin of healthy individuals and Atopic Dermatitis patients via EVs. Finally, future studies will unravel the role of CLCA2 and RBM3 in the pathogenesis of other human skin diseases associated with defects in keratinocytes.

AUTHOR CONTRIBUTIONS

Kristin Seltmann: Conceptualization (equal); data curation (equal); formal analysis (lead); funding acquisition (supporting); investigation (lead); methodology (supporting); project administration (equal); supervision (equal); validation (equal); visualization (lead); writing—original draft (equal); writing—review and editing (equal). **Britta Hettich**: Investigation (supporting); methodology (supporting); writing—review and editing (supporting). **Seraina Abele**: Formal analysis (supporting); investigation (supporting); visualization (supporting); writing—review and editing (supporting). **Selina Gurri**: Formal analysis (supporting); investigation (supporting); validation (supporting); writing—review and editing (supporting). **Valeria Mantella**: Formal analysis (supporting); investigation (supporting); methodology (equal); writing—review and editing (supporting). **Jean-Christophe Leroux**: Methodology (supporting); supervision (supporting); writing—review and editing (supporting). **Sabine Werner**: Conceptualization (equal); data curation (equal); funding acquisition (lead); project administration (lead); supervision (equal); writing—original draft (equal); writing—review and editing (equal).

ACKNOWLEDGEMENTS

We thank Drs. Andrii Kuklin and Mateusz Wietecha, ETH Zurich, for invaluable help with the bioinformatics analysis, Finn Brigger, ETH Zurich, for helpful suggestions with the nanoparticle tracking analysis, Dr. Petra Boukamp, Leibniz Institute Düsseldorf,

Germany, for HaCaT keratinocytes, Dr. Hans-Dietmar Beer, University of Zurich, for human foreskin sections, Dr. Philipp Berger, Paul Scherrer Institute, Villigen, Switzerland, for the RAB5/RAB11 multicolor expression plasmid, Dr. Paolo Nanni (Functional Genomics Center Zurich) for MS/MS analysis, Dr. Roger Meier and Dr. Tobias Schwarz (ScopeM, ETH Zurich) for image processing and Dr. Ulrike Kutay, ETH Zurich, for helpful suggestions. This work was supported by grants from the Swiss National Science Foundation (310030-212212 to S.W), the ETH Zurich (Open ETH Project SKINTEGRITY.CH to S.W. and J.-C.L.) and ETH and Leopoldina postdoctoral fellowships (to K.S.). J.-C. L. and S.W. are members of the SKINTEGRITY.CH collaborative research program.

CONFLICT OF INTEREST STATEMENT

The authors report no conflict of interest.

ORCID

Sabine Werner https://orcid.org/0000-0001-7397-8710

REFERENCES

Abdel-Ghany, M., Cheng, H. C., Elble, R. C., Lin, H. Q., DiBiasio, J., & Pauli, B. U. (2003). The interacting binding domains of the beta(4) integrin and calcium-activated chloride channels (CLCAs) in metastasis. *Journal of Biological Chemistry*, *278*(49), 49406–49416. https://doi.org/10.1074/jbc.M309086200

Boukamp, P., Petrussevska, R. T., Breitkreutz, D., Hornung, J., Markham, A., & Fusenig, N. E. (1988). Normal keratinization in a spontaneously immortalized aneuploid human keratinocyte cell line. *The Journal of Cell Biology*, *106*(3), 761–771. https://www.ncbi.nlm.nih.gov/pubmed/2450098

Chavez-Munoz, C., Morse, J., Kilani, R., & Ghahary, A. (2008). Primary human keratinocytes externalize stratifin protein via exosomes. *Journal of Cellular Biochemistry*, *104*(6), 2165–2173. https://doi.org/10.1002/jcb.21774

Chen, M. K., Hsu, J. L., & Hung, M. C. (2020). Nuclear receptor tyrosine kinase transport and functions in cancer. *Receptor Tyrosine Kinases*, *147*, 59–107. https://doi.org/10.1016/bs.acr.2020.04.010

Christianson, H. C., Svensson, K. J., van Kuppevelt, T. H., Li, J. P., & Belting, M. (2013). Cancer cell exosomes depend on cell-surface heparan sulfate proteoglycans for their internalization and functional activity. *PNAS*, *110*(43), 17380–17385. https://doi.org/10.1073/pnas.1304266110

Chung, E., Cook, P. W., Parkos, C. A., Park, Y. K., Pittelkow, M. R., & Coffey, R. J. (2005). Amphiregulin causes functional downregulation of adherens junctions in psoriasis. *The Journal of Investigative Dermatology*, *124*(6), 1134–1140. https://doi.org/10.1111/j.0022-202X.2005.23762.x

Corbeil, D., Santos, M. E., Karbanova, J., Kurth, T., Rappa, G., & Lorico, A. (2020). Uptake and fate of extracellular membrane vesicles: Nucleoplasmic reticulum-associated late endosomes as a new gate to intercellular communication. *Cells*, *9*(9), 1931. https://doi.org/10.3390/cells9091931

Dresios, J., Aschrafi, A., Owens, G. C., Vanderklish, P. W., Edelman, G. M., & Mauro, V. P. (2005). Cold stress-induced protein Rbm3 binds 60S ribosomal subunits, alters rnicroRNA levels, and enhances global protein synthesis. *Proceedings of the National Academy of Sciences of the United States of America*, *102*(6), 1865–1870. https://doi.org/10.1073/pnas.0409764102

Elble, R. C., Walia, V., Cheng, H. C., Connon, C. J., Mundhenk, L., Gruber, A. D., & Pauli, B. U. (2006). The putative chloride channel hCLCA2 has a single C-terminal transmembrane segment. *Journal of Biological Chemistry*, *281*(40), 29448–29454. https://doi.org/10.1074/jbc.M605919200

Fan, S. J., Kroeger, B., Marie, P. P., Bridges, E. M., Mason, J. D., McCormick, K., Zois, C. E., Sheldon, H., Alham, N. K., Johnson, E., Ellis, M., Stefana, M. I., Mendes, C. C., Wainwright, S. M., Cunningham, C., Hamdy, F. C., Morris, J. F., Harris, A. L., Wilson, C., & Goberdhan, D. C. I. (2020). Glutamine deprivation alters the origin and function of cancer cell exosomes. *Embo Journal*, *39*(16), e103009. https://doi.org/10.15252/embj.2019103009

Furukawa, F., Takigawa, M., Matsuyoshi, N., Shirahama, S., Wakita, H., Fujita, M., Horiguchi, Y., & Imamura, S. (1994). Cadherins in cutaneous biology. *Journal of Dermatology*, *21*(11), 802–813. https://doi.org/10.1111/j.1346-8138.1994.tb03294.x

Hettich, B. F., Greenwald, M. B.-Y., Sabine, W., & Leroux, J. C (2020). Exosomes for wound healing: Purification optimization and identification of bioactive components. *Advanced Science (Weinheim)*, *7*(23), 2002596. https://doi.org/10.1002/advs.202002596

Hu, Y. J., Liu, Y., Quan, X., Fan, W. X., Xu, B., & Li, S. Z. (2022). RBM3 is an outstanding cold shock protein with multiple physiological functions beyond hypothermia. *Journal of Cellular Physiology*, *237*(10), 3788–3802. https://doi.org/10.1002/jcp.30852

Kopp, M. R. G., Linsenmeier, M., Hettich, B., Prantl, S., Stavrakis, S., Leroux, J. C., & Arosio, P. (2020). Microfluidic shrinking droplet concentrator for analyte detection and phase separation of protein solutions. *Analytical Chemistry*, *92*(8), 5803–5812. https://doi.org/10.1021/acs.analchem.9b05329

Kriz, A., Schmid, K., Baumgartner, N., Ziegler, U., Berger, I., Ballmer-Hofer, K., & Berger, P. (2010). A plasmid-based multigene expression system for mammalian cells. *Nature Communications*, *1*, 120. https://doi.org/10.1038/ncomms1120

Kugeratski, F. G., Hodge, K., Lilla, S., McAndrews, K. M., Zhou, X., Hwang, R. F., Zanivan, S., & Kalluri, R. (2021). Quantitative proteomics identifies the core proteome of exosomes with syntenin-1 as the highest abundant protein and a putative universal biomarker. *Nature Cell Biology*, *23*(6), 631–641. https://doi.org/10.1038/s41556-021-00693-y

Liu, S. Y., Ge, D., Chen, L. N., Zhao, J., Su, L., Zhang, S. L., Miao, J. Y., & Zhao, B. X. (2016). A small molecule induces integrin beta4 nuclear translocation and apoptosis selectively in cancer cells with high expression of integrin beta4. *Oncotarget*, *7*(13), 16282–16296. https://doi.org/10.18632/oncotarget.7646

Liu, Y., Shi, H., Hu, Y., Yao, R., Liu, P., Yang, Y., & Li, S. (2022). RNA binding motif protein 3 (RBM3) promotes protein kinase B (AKT) activation to enhance glucose metabolism and reduce apoptosis in skeletal muscle of mice under acute cold exposure. *Cell Stress & Chaperones*, *27*(6), 603–618. https://doi.org/10.1007/s12192-022-01297-7

Lo Cicero, A., Delevoye, C., Gilles-Marsens, F., Loew, D., Dingli, F., Guere, C., Andre, N., Vie, K., van Niel, G., & Raposo, G. (2015). Exosomes released by keratinocytes modulate melanocyte pigmentation. *Nature Communications*, *6*, 7506. https://doi.org/10.1038/ncomms8506

Luga, V., Zhang, L., Viloria-Petit, A. M., Ogunjimi, A. A., Inanlou, M. R., Chiu, E., Buchanan, M., Hosein, A. N., Basik, M., & Wrana, J. L. (2012). Exosomes mediate stromal mobilization of autocrine Wnt-PCP signaling in breast cancer cell migration. *Cell*, *151*(7), 1542–1556. https://doi.org/10.1016/j.cell.2012.11.024

Mathieu, M., Martin-Jaular, L., Lavieu, G., & Thery, C. (2019). Specificities of secretion and uptake of exosomes and other extracellular vesicles for cell-to-cell communication. *Nature Cell Biology*, *21*(1), 9–17. https://doi.org/10.1038/s41556-018-0250-9

Mathivanan, S., Ji, H., & Simpson, R. J. (2010). Exosomes: Extracellular organelles important in intercellular communication. *Journal of Proteomics*, *73*(10), 1907–1920. https://doi.org/10.1016/j.jprot.2010.06.006

Mavrogonatou, E., Papadimitriou, K., Urban, J. P., Papadopoulos, V., & Kletsas, D. (2015). Deficiency in the alpha1 subunit of Na+/K+-ATPase enhances the anti-proliferative effect of high osmolality in nucleus pulposus intervertebral disc cells. *Journal of Cellular Physiology*, *230*(12), 3037–3048. https://doi.org/10.1002/jcp.25040

Mellacheruvu, D., Wright, Z., Couzens, A. L., Lambert, J. P., St-Denis, N. A., Li, T., Miteva, Y. V., Hauri, S., Sardiu, M. E., Low, T. Y., Halim, V. A., Bagshaw, R. D., Hubner, N. C., Al-Hakim, A., Bouchard, A., Faubert, D., Fermin, D., Dunham, W. H., Goudreault, M., … Nesvizhskii, A. I. (2013). The CRAPome: A contaminant repository for affinity purification-mass spectrometry data. *Nature Methods*, *10*(8), 730–736. https://doi.org/10.1038/nmeth.2557

Mosimann, C., Hausmann, G., & Basler, K. (2009). Beta-catenin hits chromatin: Regulation of Wnt target gene activation. *Nature Reviews. Molecular Cell Biology*, *10*(4), 276–286. https://doi.org/10.1038/nrm2654

Ou, C. Y., Kim, J. H., Yang, C. K., & Stallcup, M. R. (2009). Requirement of cell cycle and apoptosis regulator 1 for target gene activation by Wnt and beta-catenin and for anchorage-independent growth of human colon carcinoma cells. *Journal of Biological Chemistry*, *284*(31), 20629–20637. https://doi.org/10.1074/jbc.M109.014332

Proksch, E., Brandner, J. M., & Jensen, J. M. (2008). The skin: An indispensable barrier. *Experimental Dermatology*, *17*(12), 1063–1072. http://www.ncbi.nlm.nih.gov/pubmed/19043850

Proksch, E., Folster-Holst, R., & Jensen, J. M. (2006). Skin barrier function, epidermal proliferation and differentiation in eczema. *Journal of Dermatological Science*, *43*(3), 159–169. https://doi.org/10.1016/j.jdermsci.2006.06.003

Ramena, G., Yin, Y., Yu, Y., Walia, V., & Elble, R. C. (2016). CLCA2 Interactor EVA1 Is Required for Mammary Epithelial Cell Differentiation. *PLoS ONE*, *11*(3), e0147489. https://doi.org/10.1371/journal.pone.0147489

Rappa, G., Santos, M. F., Green, T. M., Karbanova, J., Hassler, J., Bai, Y. S., Barsky, S. H., Corbeil, D., & Lorico, A. (2017). Nuclear transport of cancer extracellular vesicle-derived biomaterials through nuclear envelope invagination-associated late endosomes. *Oncotarget*, *8*(9), 14443–14461. https://doi.org/10.18632/oncotarget.14804

Read, J., Ingram, A., Saleh, H. A. A., Platko, K., Gabriel, K., Kapoor, A., Pinthus, J., Majeed, F., Qureshi, T., & Al-Nedawi, K. (2017). Nuclear transportation of exogenous epidermal growth factor receptor and androgen receptor via extracellular vesicles (vol 70, pg 62, 2017). *European Journal of Cancer*, *83*, 335–335. https://doi.org/10.1016/j.ejca.2017.07.009

Sasaki, Y., Koyama, R., Maruyama, R., Hirano, T., Tamura, M., Sugisaka, J., Suzuki, H., Idogawa, M., Shinomura, Y., & Tokino, T. (2012). CLCA2, a target of the p53 family, negatively regulates cancer cell migration and invasion. *Cancer Biology & Therapy*, *13*(14), 1512–1521. https://doi.org/10.4161/cbt.22280

Savina, A., Fader, C. M., Damiani, M. T., & Colombo, M. I. (2005). Rab11 promotes docking and fusion of multivesicular bodies in a calcium-dependent manner. *Traffic (Copenhagen, Denmark)*, *6*(2), 131–143. https://doi.org/10.1111/j.1600-0854.2004.00257.x

Seltmann, K., Cheng, F., Wiche, G., Eriksson, J. E., & Magin, T. M. (2015). Keratins stabilize hemidesmosomes through regulation of beta4-integrin turnover. *The Journal of investigative dermatology*, *135*(6), 1609–1620. https://doi.org/10.1038/jid.2015.46

Seltmann, K., Meyer, M., Sulcova, J., Kockmann, T., Wehkamp, U., Weidinger, S., Auf dem Keller, U., & Werner, S. (2018). Humidity-regulated CLCA2 protects the epidermis from hyperosmotic stress. *Science Translational Medicine*, *10*(440), eaao4650. https://doi.org/10.1126/scitranslmed.aao4650

Seltmann, K., Roth, W., Kroger, C., Loschke, F., Lederer, M., Huttelmaier, S., & Magin, T. M. (2013). Keratins mediate localization of hemidesmosomes and repress cell motility. *The Journal of investigative dermatology*, *133*(1), 181–190. https://doi.org/10.1038/jid.2012.256

Shah, P., Chaumet, A., Royle, S. J., & Bard, F. A. (2019). The NAE pathway: Autobahn to the nucleus for cell surface receptors. *Cells*, *8*(8), 915. https://doi.org/10.3390/cells8080915

Stojadinovic, O., Brem, H., Vouthounis, C., Lee, B., Fallon, J., Stallcup, M., Merchant, A., Galiano, R. D., & Tomic-Canic, M. (2005). Molecular pathogenesis of chronic wounds: The role of beta-catenin and c-myc in the inhibition of epithelialization and wound healing. *American Journal of Pathology*, *167*(1), 59–69. https://doi.org/10.1016/s0002-9440(10)62953-7

Sun, J., Zhang, T., Cheng, M., Hong, L., Zhang, C., Xie, M., Sun, P., Fan, R., Wang, Z., Wang, L., & Zhong, J. (2019). TRIM29 facilitates the epithelial-to-mesenchymal transition and the progression of colorectal cancer via the activation of the Wnt/beta-catenin signaling pathway. *Journal of Experimental & Clinical Cancer Research*, *38*(1), 104. https://doi.org/10.1186/s13046-019-1098-y

Teo, G., Liu, G., Zhang, J., Nesvizhskii, A. I., Gingras, A. C., & Choi, H. (2014). SAINTexpress: Improvements and additional features in Significance Analysis of INTeractome software. *Journal of Proteomics*, *100*, 37–43. https://doi.org/10.1016/j.jprot.2013.10.023

Veeman, M. T., Slusarski, D. C., Kaykas, A., Louie, S. H., & Moon, R. T. (2003). Zebrafish prickle, a modulator of noncanonical Wnt/Fz signaling, regulates gastrulation movements. *Current Biology*, *13*(8), 680–685. https://doi.org/10.1016/S0960-9822(03)00240-9

Venugopal, A., Subramaniam, D., Balmaceda, J., Roy, B., Dixon, D. A., Umar, S., Weir, S. J., & Anant, S. (2016). RNA binding protein RBM3 increases beta-catenin signaling to increase stem cell characteristics in colorectal cancer cells. *Molecular Carcinogenesis*, *55*(11), 1503–1516. https://doi.org/10.1002/mc.22404

Walde, S., Thakar, K., Hutten, S., Spillner, C., Nath, A., Rothbauer, U., Wiemann, S., & Kehlenbach, R. H. (2012). The nucleoporin Nup358/RanBP2 promotes nuclear import in a cargo- and transport receptor-specific manner. *Traffic (Copenhagen, Denmark)*, *13*(2), 218–233. https://doi.org/10.1111/j.1600-0854.2011.01302.x

Walia, V., Yu, Y., Cao, D., Sun, M., McLean, J. R., Hollier, B. G., Cheng, J., Mani, S. A., Rao, K., Premkumar, L., & Elble, R. C. (2012). Loss of breast epithelial marker hCLCA2 promotes epithelial-to-mesenchymal transition and indicates higher risk of metastasis. *Oncogene*, *31*(17), 2237–2246. https://doi.org/10.1038/onc.2011.392

Wellmann, S., Truss, M., Bruder, E., Tornillo, L., Zelmer, A., Seeger, K., & Buhrer, C. (2010). The RNA-binding protein RBM3 is required for cell proliferation and protects against serum deprivation-induced cell death. *Pediatric Research*, *67*(1), 35–41. https://doi.org/10.1203/PDR.0b013e3181c13326

Welsh, J. A., Arkesteijn, G. J. A., Bremer, M., Cimorelli, M., Dignat-George, F., Giebel, B., Gorgens, A., Hendrix, A., Kuiper, M., Lacroix, R., Lannigan, J., van Leeuwen, T. G., Lozano-Andres, E., Rao, S., Robert, S., de Rond, L., Tang, V. A., Tertel, T., Yan, X., … van der Pol, E. (2023). A compendium of single extracellular vesicle flow cytometry. *Journal of Extracellular Vesicles*, *12*(2), e12299. https://doi.org/10.1002/jev2.12299

Welsh, J. A., Goberdhan, D. C., O'Driscoll, L., Thery, C., & Witwer, K. W. (2024). MISEV2023: An updated guide to EV research and applications. *Journal of Extracellular Vesicles*, *13*(2), e12416. https://doi.org/10.1002/jev2.12416

Xu, R., Hu, J., Zhang, T., Jiang, C., & Wang, H. Y. (2016). TRIM29 overexpression is associated with poor prognosis and promotes tumor progression by activating Wnt/beta-catenin pathway in cervical cancer. *Oncotarget*, *7*(19), 28579–28591. https://doi.org/10.18632/oncotarget.8686

Zeng, Y., Wodzenski, D., Gao, D., Shiraishi, T., Terada, N., Li, Y. Q., Griend, D. J. V., Luo, J., Kong, C. Z., Getzenberg, R. H., & Kulkarni, P. (2013). Stress-response protein RBM3 attenuates the stem-like properties of prostate cancer cells by interfering with CD44 variant splicing. *Cancer Research*, *73*(13), 4123–4133. https://doi.org/10.1158/0008-5472.Can-12-1343

Zhang, B., Wang, M., Gong, A. H., Zhang, X., Wu, X. D., Zhu, Y. H., Shi, H., Wu, L. J., Zhu, W., Qian, H., & Xu, W. R. (2015). HucMSC-exosome mediated-Wnt4 signaling is required for cutaneous wound healing. *Stem Cells*, *33*(7), 2158–2168. https://doi.org/10.1002/stem.1771

Zhu, X., Jia, W., Yan, Y., Huang, Y., & Wang, B. (2021). NOP14 regulates the growth, migration, and invasion of colorectal cancer cells by modulating the NRIP1/GSK-3beta/beta-catenin signaling pathway. *European Journal of Histochemistry*, *65*(3), 3246. https://doi.org/10.4081/ejh.2021.3246

Zhu, X. Z., Buhrer, C., & Wellmann, S. (2016). Cold-inducible proteins CIRP and RBM3, a unique couple with activities far beyond the cold. *Cellular and Molecular Life Sciences*, *73*(20), 3839–3859. https://doi.org/10.1007/s00018-016-2253-7

SUPPORTING INFORMATION

Additional supporting information can be found online in the Supporting Information section at the end of this article.

How to cite this article: Seltmann, K., Hettich, B., Abele, S., Gurri, S., Mantella, V., Leroux, J.-C., & Werner, S. (2024). Transport of CLCA2 to the nucleus by extracellular vesicles controls keratinocyte survival and migration. *Journal of Extracellular Vesicles*, *13*, e12430. https://doi.org/10.1002/jev2.12430